Cell Reports

Article

Heterotypic phase separation of Hfq is linked to its roles as an RNA chaperone

Graphical abstract

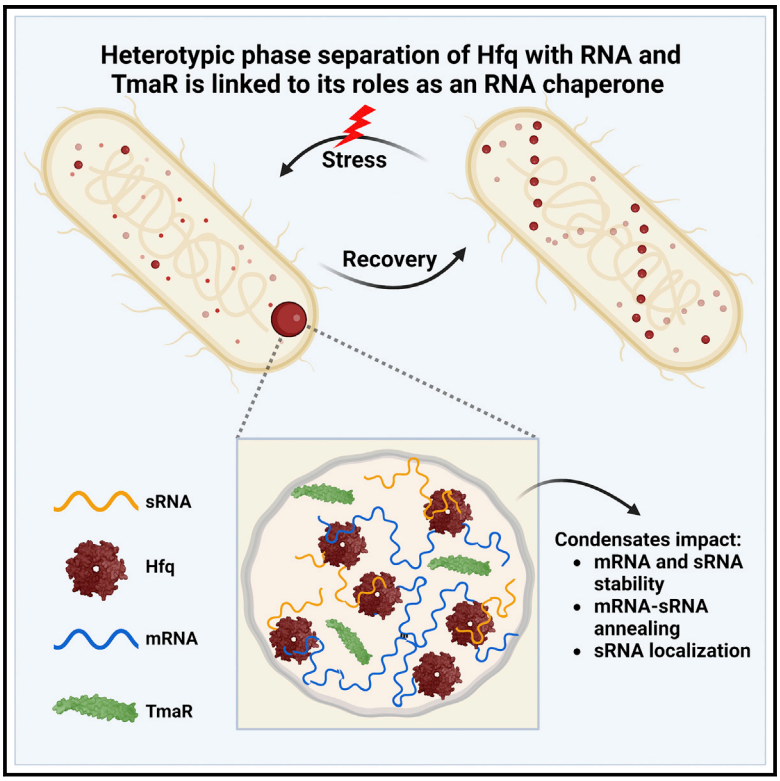

Highlights

- Hfq undergoes phase separation via heterotypic interactions with RNA
- Hfq forms condensates of different material states in stressed and unstressed cells
- Phase separation of Hfq depends on the pole-localizer TmaR
- Phase separation of Hfq correlates with its activity as an RNA chaperone

Authors

Omer Goldberger, Tamar Szoke, Anat Nussbaum-Shochat, Orna Amster-Choder

Correspondence

ornaam@ekmd.huji.ac.il

In brief

Hfq is an RNA chaperon that binds to small regulatory RNAs (sRNAs) and matches them with mRNAs, thus regulating their fate. Goldberger et al. show that, upon stress, Hfq undergoes phase separation and condenses at the cell poles with RNA. This process is important for its role as sRNA-mRNA matchmaker.

Goldberger et al., 2022, Cell Reports *41*, 111881
December 27, 2022
https://doi.org/10.1016/j.celrep.2022.111881

CellPress

Cell Reports

CellPress
OPEN ACCESS

Article

Heterotypic phase separation of Hfq is linked to its roles as an RNA chaperone

Omer Goldberger,[1] Tamar Szoke,[1] Anat Nussbaum-Shochat,[1] and Orna Amster-Choder[1,2,*]
[1]Department of Microbiology and Molecular Genetics, IMRIC, The Hebrew University Faculty of Medicine, P.O. Box 12272, Jerusalem 91120, Israel
[2]Lead contact
*Correspondence: ornaam@ekmd.huji.ac.il
https://doi.org/10.1016/j.celrep.2022.111881

SUMMARY

Hfq, an Sm-like protein and the major RNA chaperone in *E. coli*, has been shown to distribute non-uniformly along a helical path under normal growth conditions and to relocate to the cell poles under certain stress conditions. We have previously shown that Hfq relocation to the poles is accompanied by polar accumulation of most small RNAs (sRNAs). Here, we show that Hfq undergoes RNA-dependent phase separation to form cytoplasmic or polar condensates of different density under normal and stress conditions, respectively. Purified Hfq forms droplets in the presence of crowding agents or RNA, indicating that its condensation is via heterotypic interactions. Stress-induced relocation of Hfq condensates and sRNAs to the poles depends on the pole-localizer TmaR. Phase separation of Hfq correlates with its ability to perform its posttranscriptional roles as sRNA-stabilizer and sRNA-mRNA matchmaker. Our study offers a spatiotemporal mechanism for sRNA-mediated regulation in response to environmental changes.

INTRODUCTION

To occupy diverse niches, bacteria have adopted strategies for sensing and coping with environmental changes, which may be global or specific to a stressor and may involve various proteinaceous and RNA components.[1] Many of these strategies involve regulation of gene expression mediated by small RNA (sRNA) molecules.[2,3] sRNAs have been intensively studied in a wide array of bacterial species and shown to contribute to posttranscriptional control by pairing with target mRNAs.[4] These interactions between a conserved seed sequence within the sRNA and a target sequence within the mRNA can lead to decrease or increase in protein expression, with the former appearing to be more common. The differential expression of sRNAs and their positive or negative effect on their mRNA targets creates a complex network[5,6] that generates adequate responses.

Several RNA chaperones mediate the sRNA-mRNA interactions and stabilize the sRNAs, among them ProQ, CsrA, and Hfq.[7] Hfq, the major RNA chaperone in *E. coli*, is an Sm-like protein, sharing a ring-like structure with the eukaryotic RNA-binding Sm proteins.[8] Hfq forms a homohexameric ring, and crystallography studies revealed three distinct surfaces on the Hfq hexamer, each bearing a unique motif and, hence, exhibiting different sequence affinities.[9] Hfq distal face binds mostly mRNAs via an ARN motif, its proximal face binds mainly to sRNAs via the U-rich sequences present at the 3′ end of the Rho-independent terminators of these molecules,[10] whereas its rim (lateral) face can bind and stabilize molecules via UA-rich sites.[10] A thorough examination of Hfq mutants with single base substitutions established the contribution of each region to binding of sRNA/mRNA and to the chaperone activity.[9,10] Moreover, in recent studies, Hfq was shown to bind additional substrates, i.e., DNA, tRNAs, and rRNAs.[11] These findings explain the pleiotropic effects observed in *E. coli* and *Salmonella* upon deletion of the *hfq* gene, including decreased cell growth[12] and reduced biofilm formation.[13]

Hfq has been suggested to localize near the bacterial membrane by electron microscopy.[14] Using fluorescent immunostaining, Hfq has been visualized in foci distributed non-uniformly along a helical path under normal growth conditions,[15] a pattern depending on its C-terminal domain.[16] By means of single-molecule super-resolution, a similar subcellular distribution has been detected, which was completely abolished using the transcription inhibitor rifampicin. As opposed to its helical pattern under native conditions, we have previously shown that, during high osmolarity, Hfq relocates to clusters at the *E. coli* cell poles, where most sRNAs accumulate in an Hfq-dependent manner.[17] Hfq was shown to localize to the poles also under long-term nitrogen starvation together with the degradosome components,[18,19] although its role under this stress is unknown, nor are sRNAs related to this stress known. Based on partial dispersal of these polar foci in 1,6-hexanediol, it has been speculated that they might assemble by phase separation.[19]

Localization of RNA-binding proteins (RBPs) is expected to have various regulatory implications and is intuitively expected to be linked to the localization of the RNAs they bind. Indeed, the polar accumulation of sRNAs upon high osmolarity was lost in an Hfq deletion strain.[17] Recently, phase separation has

been shown to provide a mechanism for the formation of local condensates containing RNA-binding sites (RBSs) and their bound RNAs in eukaryotes,[20] as well as in one case in bacteria.[21] Phase separation has been implicated in the formation of membraneless organelles in eukaryotes and in human pathologies, caused by transition of proteins to a solid-like phase.[22] New studies suggest that bacteria also organize their cytoplasm by phase separation-mediated formation of micro-compartments,[23,24] providing a way for compartmentalization of macromolecules in the alleged non-compartmentalized bacterial cell. Examples include the *Caulobacter crescentus* RNase E, which forms condensates with RNAs,[21] the assemblage of signaling proteins in a polar membraneless organelle in this organism,[25] and the *E. coli* cell division protein FtsZ, which forms phase-separated condensates with its nucleoid-associated inhibitor SlmA.[26] However, the strategies used by bacteria for the establishment of phase separation-driven membraneless organelles are largely unknown. The role of RNA in condensates is under extensive study, with an emerging recognition that not only does the nucleic acid sequence matter, but also the structure plays an important role.[27] Still, the mechanisms underlying condensate assembly have not been fully characterized.

In this study, we show that the major RNA chaperone, Hfq, forms biomolecular condensates under high salt stress and nutrient deprivation conditions via heterotypic interactions with RNA. The process of Hfq condensation and the dynamic behavior of the condensates were characterized in the cell and with the purified protein. Phase separation of Hfq depends on RNA both *in vivo* and *in vitro*. Formation of Hfq condensates in both stressed and unstressed cells and the increase in the level of sRNAs under stress depend on TmaR, a polar protein recently shown by us to control the activity of the major regulator of sugar metabolism by polar sequestration and release[28] and to phase separation.[29] Our results strongly recommend that the material state of Hfq foci, whether in the cytoplasm or at the poles, is important for its activities as a posttranscriptional regulator.

RESULTS

Hfq forms biomolecular condensates of different material states in the cytoplasm and at the poles

The recent findings that Hfq relocates from the non-uniformly distributed foci, observed under normal physiological conditions, to the cell poles upon specific stresses, and the dependence of polar accumulation of sRNAs on this phenomenon,[17] prompted us to further explore the spatiotemporal distribution of Hfq and its relation with RNA localization. To monitor Hfq localization in live cells, we constructed a strain expressing Hfq fused to mCherry under its native regulatory elements. Functionality of the chimeric protein in regulating mRNA levels and sRNA stability was shown to be comparable with that of untagged Hfq by measuring the levels of SgrS sRNA and its mRNA target *yigL*[30,31] under sugar toxicity by qRT-PCR (Figure S1A), as described before,[32] and by comparing its ability to mediate positive and negative regulation of mRNAs in the presence of their cognate sRNAs (Figure S1B), as described previously.[33] In addition, replacement of the *hfq* gene by *hfq-mCherry* did not bring about any fitness cost for the cell, as deduced from the almost identical growth curves of cells expressing it and cells expressing untagged Hfq (Figure S1C). Since polar localization of Hfq under osmotic stress was previously demonstrated in the presence of high sucrose by immunostaining,[17] we first monitored Hfq-mCherry localization in the presence of a different osmotic stressor, high salt. The rate of polar clusters formation by Hfq-mCherry under high salt (Figure S2) was comparable with the rate reported for Hfq in the presence of high sucrose,[17] indicating that the mCherry tag does not affect Hfq localization. Of note, the punctate appearance of Hfq along a helical path in unstressed cells, which is characteristic of large complexes that spatially segregate from the helical nucleoid, indicates that Hfq, probably bound to RNA molecules, forms clusters also in the cytoplasm. Interestingly, this pattern is abolished in the mock-treated cells upon entry to stationary phase (SP) (Figure S2, upper panel, after 4 h), and Hfq becomes homogenously distributed in the cytoplasm, raising the possibility that a significant fraction of Hfq released the RNA at that stage.

Next, we aimed at examining Hfq-mCherry localization pattern in cells exposed to additional stresses, starting with nutrient deprivation during late SP. Therefore, we examined Hfq-mCherry distribution in cells grown overnight and detected it mainly at the cell poles (Figure 1A). Of note, *E. coli* cells in late SP are smaller in size than cells in logarithmic phase. To validate the accumulation of Hfq in polar foci in late SP, we used immunostaining to monitor localization of FLAG-tagged Hfq, previously shown to be functional.[5] A distinct, mostly polar cluster of Hfq-FLAG was observed in cells in late SP (Figure 1B). Cluster formation in late SP was not due to a change in cellular Hfq levels, as validated in western blot analysis (Figure S3A). It was also not due to the mCherry tag, since mCherry expressed from the same locus in the chromosome was observed as evenly distributed within the cell (Figure S3B). Importantly, Hfq-mCherry clusters are not aggregates, as demonstrated by co-expressing it with the inclusion body-binding protein A (IbpA), a reporter for the presence of aggregated proteins,[34] tagged with msfGFP (Figure S4A). Of note, IbpA-msfGFP in cells expressing Hfq-mCherry was hardly expressed and was completely segregated from Hfq-mCherry in the few cells expressing it. Finally, Hfq assemblage at the poles is not due to nucleoid occlusion, since condensing the chromosome by the addition of chloramphenicol did not affect the formation of Hfq polar foci (Figure S4B). Hence, Hfq relocates to the poles and clusters there in cells in late SP. On the other hand, Hfq did not localize to the poles of cells exposed to oxidative or iron limitation stresses for the same time that leads to polar accumulation of Hfq exposed to high osmolarity (Figure S2). To further investigate the cause for Hfq clustering, we tested foci formation in cells grown in minimal medium with a defined carbon source (glucose or succinate) or in conditioned medium (filtered medium of overnight grown cells). The results in Figure S5 show that growth in minimal medium, regardless of the carbon source, did not result in Hfq condensation at a shorter time than growth in rich medium (Figure S5, top and middle panels), ruling out the possibility that carbon might have been the nutrient that has been exhausted after overnight growth, and in line with a previous observation.[18] In

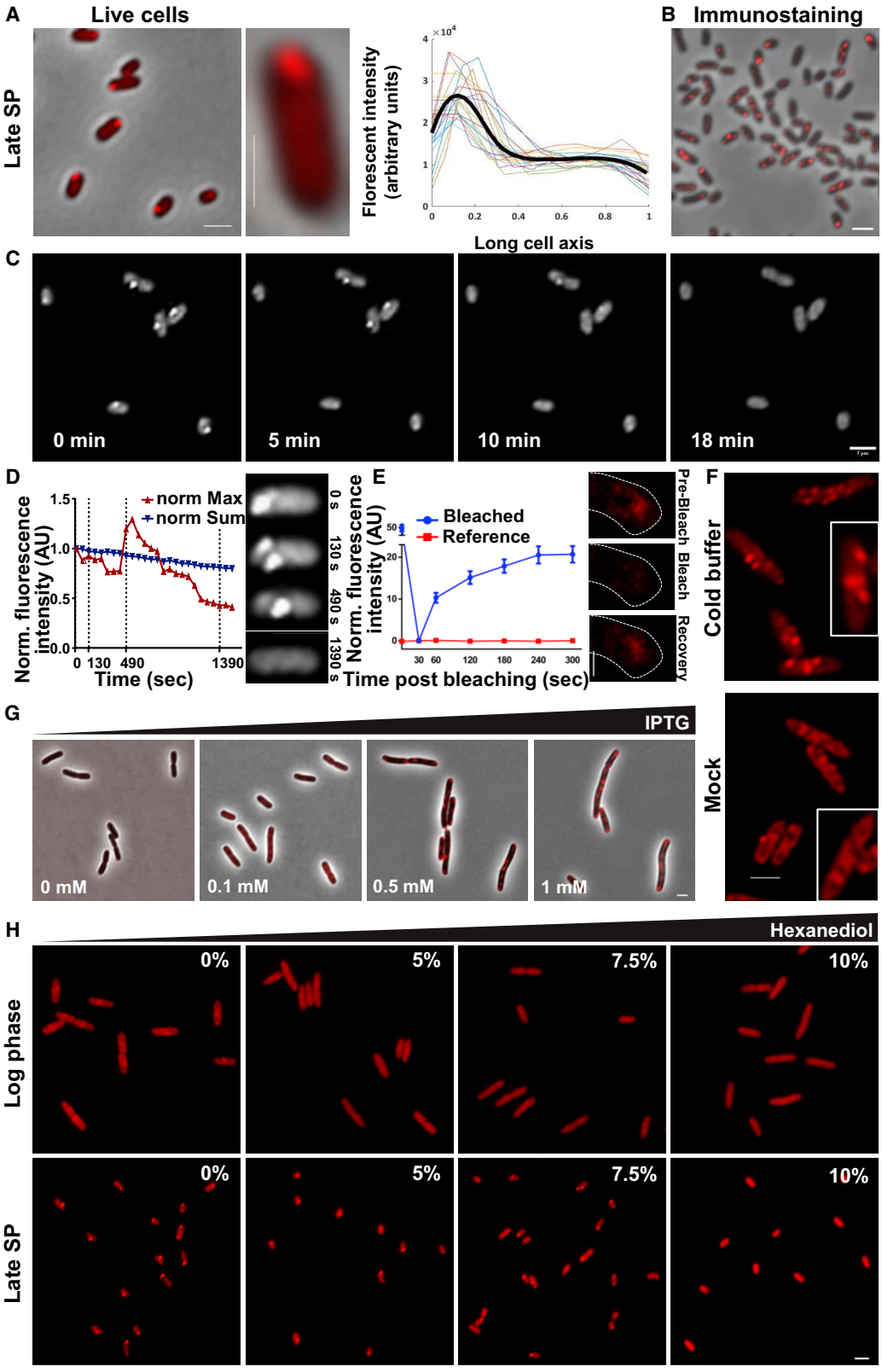

(legend on next page)

addition, we observed rapid increase in cluster formation upon growth in conditioned medium (Figure S5, bottom panels), supporting the notion that this medium lacks important nutrient/s, although the presence of a secreted signal molecule in the used medium cannot be ruled out. Summarily, relocation of Hfq to the poles becomes manifested under certain stresses, but not others.

Both the typical punctate distribution of Hfq that follows a helical path in exponential phase cells and its accumulation in polar clusters during certain stresses raised the possibility that Hfq undergoes phase separation to form biomolecular condensates. To determine if Hfq phase separates, we tested several hallmark parameters that characterize the behavior of proteins that undergo phase separation *in vivo* as follows. The dynamics of Hfq polar clusters and the dissolution as a function of cellular state was demonstrated by their dispersal in cells recovering from late SP (Figure 1C; Video S1). The characterized fast and reversible fusing and splitting events were documented by fluorescence microscopy (Figure 1D; Video S2). The dynamics of Hfq condensates was also exhibited by their recovery shortly after bleaching in a fluorescent recovery after photobleaching (FRAP) experiment (Figure 1E; Video S3). Hence, Hfq cluster dynamics is in accord with the behavior reported for phase separation condensates.[35]

Phase separation-driven condensates were reported to often form at low temperatures.[36] Indeed, cells in logarithmic phase, which were resuspended in cold medium, exhibited rapid accumulation of Hfq in foci that appeared along the helical path of Hfq distribution, as opposed to cells from the same culture resuspended in medium at room temperature (mock) (Figure 1F). Phase separation condensates also exhibit a concentration-dependent behavior.[35] To examine the influence of Hfq subcellular concentration on condensate formation, we expressed it from an inducible promoter on a plasmid. Our results show that formation of Hfq-mCherry condensates increased in an inducer concentration-dependent manner (Figures 1G, S6A, and S6B). Hence, the formation of Hfq polar condensates depends on temperature and Hfq concentration in the cell.

Next, we tested the effect of 1,6-hexanediol, an aliphatic alcohol, which has emerged as a tool to distinguish between assemblies of different material states,[35] on Hfq subcellular distribution. Due to the dramatic effect of hexanediol on growth (Figure S6C), cells were not incubated with it, but rather placed on an agar pad containing the indicted concentration and imaged instantaneously. Hexanediol led to more homogeneous distribution of Hfq, both in cells growing exponentially and in overnight grown cells (Figure 1H). Notably, cells in these two growth phases seem to exhibit different sensitivity to disruption by hexanediol, i.e., total disruption of Hfq polar foci is achieved in the presence of 10% hexanediol in late SP cells, whereas 7.5% hexanediol seems to be sufficient to disperse Hfq in exponential phase cells, which are more difficult to be detected in images acquired by regular fluorescence microscopy. These results suggest that Hfq forms condensates in both growth phases, typified by different material states, which can be different degrees of condensation in either liquid or gel membrane-less compartments.

Because proteins that undergo phase separation typically contain intrinsically disordered regions (IDRs), we analyzed the Hfq sequence by several algorithms that identify protein regions involved in phase separation.[35] PLAAC (http://plaac.wi.mit.edu/)[37] and PAPA[38] predicted that Hfq has a large IDR at its C terminus and a short one at its N terminus (Figure S7A). The existence of these two IDRs is supported by the fact that their structure could not be determined by X-ray crystallography.[16,39] Notably, the results in Figure S7 show that the C-terminal IDR (residues 72–103) is neither necessary nor sufficient for condensate formation *in vivo*, whereas the structured domain (residues 1–65), which contains the RBSs, is both necessary and sufficient for clustering, both during log phase and late SP

Figure 1. Hfq undergoes phase separation in stressed and unstressed cells

(A) Left panel: image showing polar clusters of Hfq-mCherry, obtained by live-cell microscopy, in late SP cells, which express the proteins from the native *hfq* locus in the chromosome. Approximately 90% of the cells contain a cluster. Scale bar, 2 μm. Mid panel: a representative image of a single live cell in late SP harboring an Hfq polar cluster. Scale bar, 1 μm. Right panel: fluorescence intensity profiles of 20 representative cells, expressing Hfq-mCherry, along the long cell axis after normalizing to cell length. Each cell is presented by a different color, and the average is shown by a bold black line. mCherry intensity is shown in arbitrary units.

(B) An image showing polar clusters of Hfq-FLAG obtained by immunofluorescence staining, in late SP cells, which express the protein from its native locus in the chromosome. Approximately 60% of the cells contain a cluster, regardless to its cellular location.

(C) Snapshots from time-lapse microscopy (see Video S1) showing dispersal of Hfq-mCherry clusters over time in cells recovering from nutrient deprivation in late SP. Scale bar, 2 μm.

(D) Left panel: graph of the maximum (norm max, red) and sum (norm sum, blue) florescence intensity (in arbitrary units) recorded over time and normalized to time 0 s (see Video S2). Right panel: snapshots from Video S2 showing a cell recovering from nutrient deprivation in late SP. The Hfq level in the snapshot micrographs is indicated in the florescence intensity plot by vertical dashed lines. Scale bar, 2 μm.

(E) Left panel: a graph showing fluorescence recovery of Hfq-mCherry condensates in photobleached cells (bleached, blue, n = 15) or in non-bleached cells (reference, red, n = 15) from the time of bleaching over 300 s. Quantification of the average fluorescence intensity was normalized to the pre-bleach intensity. Vertical error bars show the standard error of the mean measurement. Right panel: representative confocal micrographs of a cell before and after bleaching (see Video S3). Cell borders are marked by a dashed line. Scale bar, 0.5 μm.

(F) Images of live cells expressing Hfq-mCherry exposed to a sudden drop in temperature. Cells in log phase were mixed with PBS at either RT (mock) or 4°C (cold buffer) and immediately observed by fluorescence microscopy. Scale bar, 2 μm.

(G) Images of live cells in exponential phase expressing Hfq-mCherry from an inducible promoter on a plasmid in the presence of the indicated concentrations of IPTG inducer. Merged images of phase and mCherry channels are presented. Scale bar, 1 μm.

(H) Images of live cells in exponential growth phase (upper panel) or in late SP (lower panel) treated with the indicated hexanediol concentrations. Note that dispersal of Hfq polar clusters in starved cells is achieved at a higher hexanediol concentration compared with dispersal of Hfq cytoplasmic foci in non-starved cells (10% compared with 7.5%, respectively). Scale bar, 1 μm.

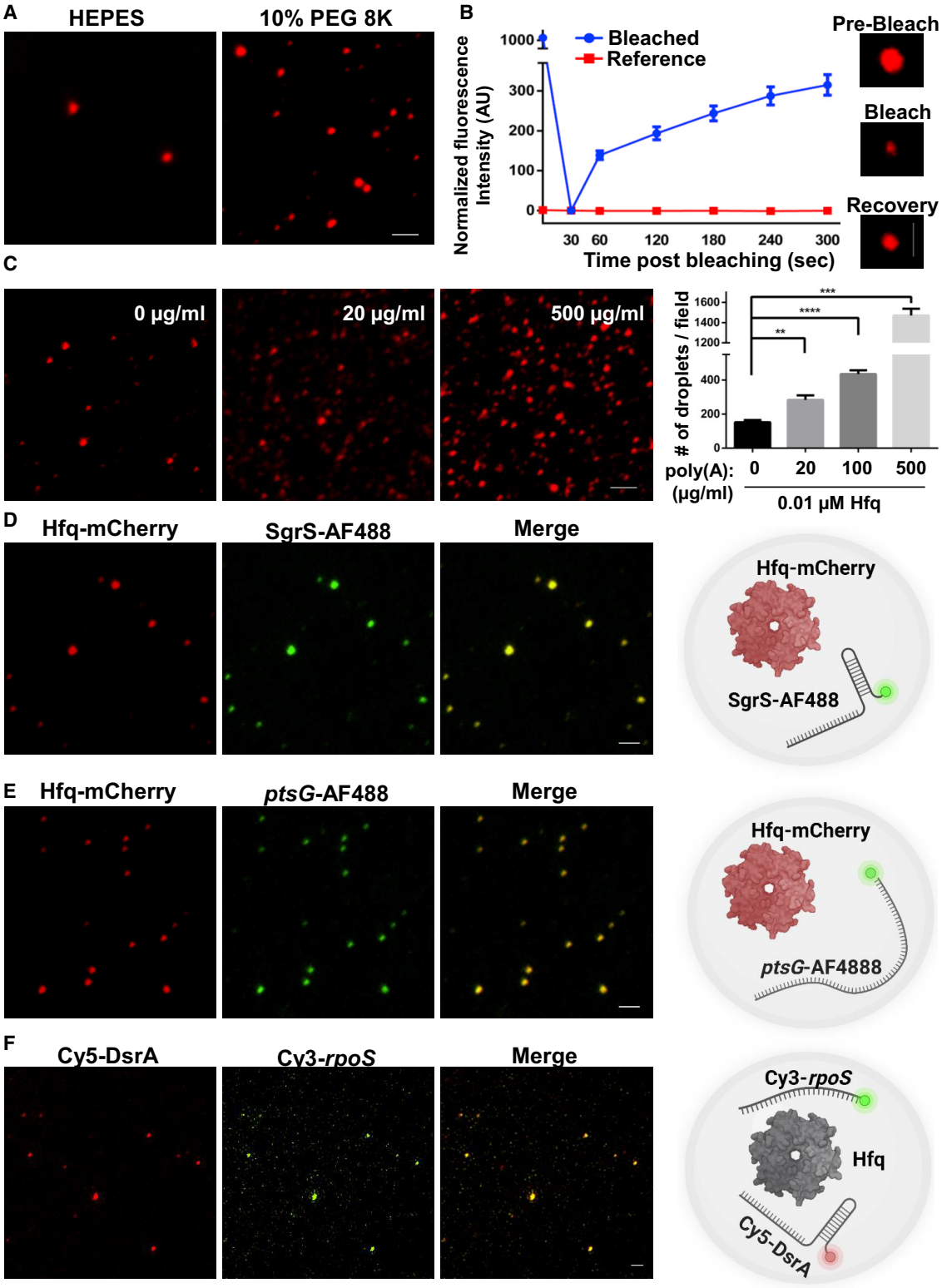

Figure 2. Droplets formation by purified Hfq is enhanced by RNA

(A) The effect of a crowding agent on the ability of purified Hfq to form droplets. Shown are representative microscopy images of purified Hfq-mCherry taken before (left image) and after (right image) the addition of 8 kDa polyethylene glycol (PEG) to purified Hfq-mCherry in HEPES buffer (150 μM NaCl), Scale bar, 2 μm. See also Figure S9A.

(legend continued on next page)

(Figure S7B, upper and lower panels, respectively). These results are line with previous documentation of the truncated Hfq protein localization.[18] Although the level of the truncated Hfq proteins, mainly that of the IDR alone, are lower than that of wild-type (WT) Hfq, when all proteins are expressed from the plasmid used to observe their condensation, they are higher or comparable with the level of Hfq expressed from the chromosome (Figure S8). Since Hfq phase separated when expressed from the chromosome or from the plasmid, the different levels cannot account for the inability of the IDR domain to phase separate. Of note, the IDR domain together with polyphosphate have been recently shown to mediate Hfq binding to DNA.[40] Finally, analysis of Hfq using the FuzDrop prediction tool (https://fuzdrop.bio.unipd.it/predictor)[41] assigns Hfq a pLLPS score of 0.9501 (pLLPS $\geq$ 0.60 suggests that the protein can spontaneously phase separate), predicting its ability to phase separate.

Taken together, our results demonstrate that Hfq forms condensates via phase separation *in vivo*, both in the absence and presence of stress, which differs in their material state.

Phase separation of purified Hfq *in vitro* requires additional factors

Examination of purified protein by *in vitro* assays sheds light on the ability of a protein to phase separate.[35] Hence, to further establish the notion that Hfq undergoes phase separation and characterizes the requirement for this process, we purified Hfq and examined its behavior under the microscope. The results in Figure S9A show that purified Hfq-mCherry, but not purified mCherry, is capable of forming droplets, the characteristic appearance of biomolecular condensates *in vitro*, but this process was efficient only in the presence of crowding agents, such as polyethylene glycol (PEG) (6 or 8 kDa) (Figures 2A and S9A). These results indicate that Hfq does not phase separate via homotypic interactions. Of note, Hfq at 500-fold higher concentration, which is significantly increased compared with Hfq physiological concentration,[42] may phase separate efficiently.[40] Increasing Hfq concentration in the presence of a crowding agent resulted in a gradual elevation in droplets formation (Figure S9B). Hence, Hfq phase separates *in vitro* in a concentration-dependent manner but requires additional factors.

Since monovalent salts have been suggested to affect condensate formation in a concentration-dependent manner,[20] we inspected purified Hfq-mCherry, at a constant concentration, in the presence of a crowding agent and increasing NaCl concentration. Condensate density continually decreased upon increasing salt concentration (Figure S9C). Adding increasing amounts of hexanediol in the presence of a constant salt concentration led to a significant additional reduction in the appearance of Hfq droplets (Figure S9D), although not competently. Together, these results suggest that weak interactions are involved in Hfq phase separation.

Dynamic behavior of purified Hfq droplets was exhibited by their merging (Figure S10A, image on the right), clearly demonstrated by the increase in the local fluorescent intensity (Figure S10A, graph on the left). Finally, a FRAP experiment was conducted, and rapid increase in the fluorescence intensity of Hfq droplets after photobleaching was recorded, as opposed to non-bleached droplets (Figure 2B). Of note, these results were obtained in the presence of PEG.

Taken together, the results thus far demonstrate that purified Hfq is capable of undergoing phase separation in the presence of crowding agents, suggesting that its phase separation in the cell requires additional factors. As previously recommended,[35] *in vitro* analyses with purified proteins should be interpreted while taking into consideration the artificial conditions. Hence, we regard the *in vitro* results as a support for the notion of Hfq phase separation observed *in vivo*.

Phase separation of purified Hfq depends on RNA and on the distal and rim faces of the Hfq hexamer

The essentiality of the RBS domain in Hfq for polar condensate formation raised the possibility that RNA is involved in Hfq phase separation, as often reported for other phase separation proteins.[27] Recent studies suggest that RNAs can affect phase separation by lowering the threshold of protein concentration required for the process. In addition, phase separation can facilitate RNA localization (reviewed in Langdon and coworkers[43,44]). Hence, phase separation offers a putative mechanism for Hfq-dependent sRNA-mRNA co-localization and coordinated regulation. To examine this possibility, we asked if RNA has an effect on phase separation of purified Hfq by adding

(B) Left panel: a graph showing fluorescence recovery of Hfq-mCherry droplets that were photobleached (bleached, blue, n = 15) or not bleached (reference, red, n = 15) from the time of bleaching over 300 s in the presence of 10% 8 kDa PEG. Quantification of the average fluorescence intensity was normalized to the pre-bleach intensity. Vertical error bars show the standard error of the mean measurement. Right panel: representative confocal micrographs of a droplet before and after bleaching. Scale bar, 1 μm.

(C) The effect of RNA on the ability of Hfq to form droplets. Shown are fluorescence microscopy images of purified Hfq-mCherry at a constant concentration before and after the addition of increasing concentrations of poly(A) (left panels) in the presence of 10% 8 kDa PEG. The bar plot shows the number of droplets formed by Hfq-mCherry per field in the different concentrations of poly(A) (right panel). Scale bar, 2.5 μm. Statistical analysis for the differences between samples was conducted using the Mann-Whitney test. The calculated p values are **0.0072, ***0.0004, and ****$p < 0.0001$.

(D) Hfq-mCherry droplets co-localization with SgrS-labeled sRNA. Representative microscopy images showing purified Hfq-mCherry (left image) and *in vitro* transcribed and labeled SgrA-AF488 sRNA (middle image) in the presence of 10% 8 kDa PEG (see control in Figure S11A). The merged image is presented on the right. Scale bar, 2 μm.

(E) Hfq-mCherry droplets co-localization with *ptsG*-labeled mRNA. Representative microscopy images of purified Hfq-mCherry (left image) and *in vitro* transcribed and labeled *ptsG*-AF488 mRNA (middle image) in the presence of 10% 8 kDa PEG (see control in Figure S11B). The merged image is presented (right image). Scale bar, 2 μm.

(F) Un-tagged purified Hfq droplets co-localization with Cy5-DsrA sRNA and Cy3-*rpoS* mRNA-labeled oligos. Representative microscopy images of Cy5-DsrA-labeled (left image) and Cy3-*rpoS*-labeled (middle image) oligos mixed with un-tagged Hfq in the presence of 10% 8 kDa PEG, (see control in Figure S12B). The merged image is presented (right image). Scale bar, 2 μm.

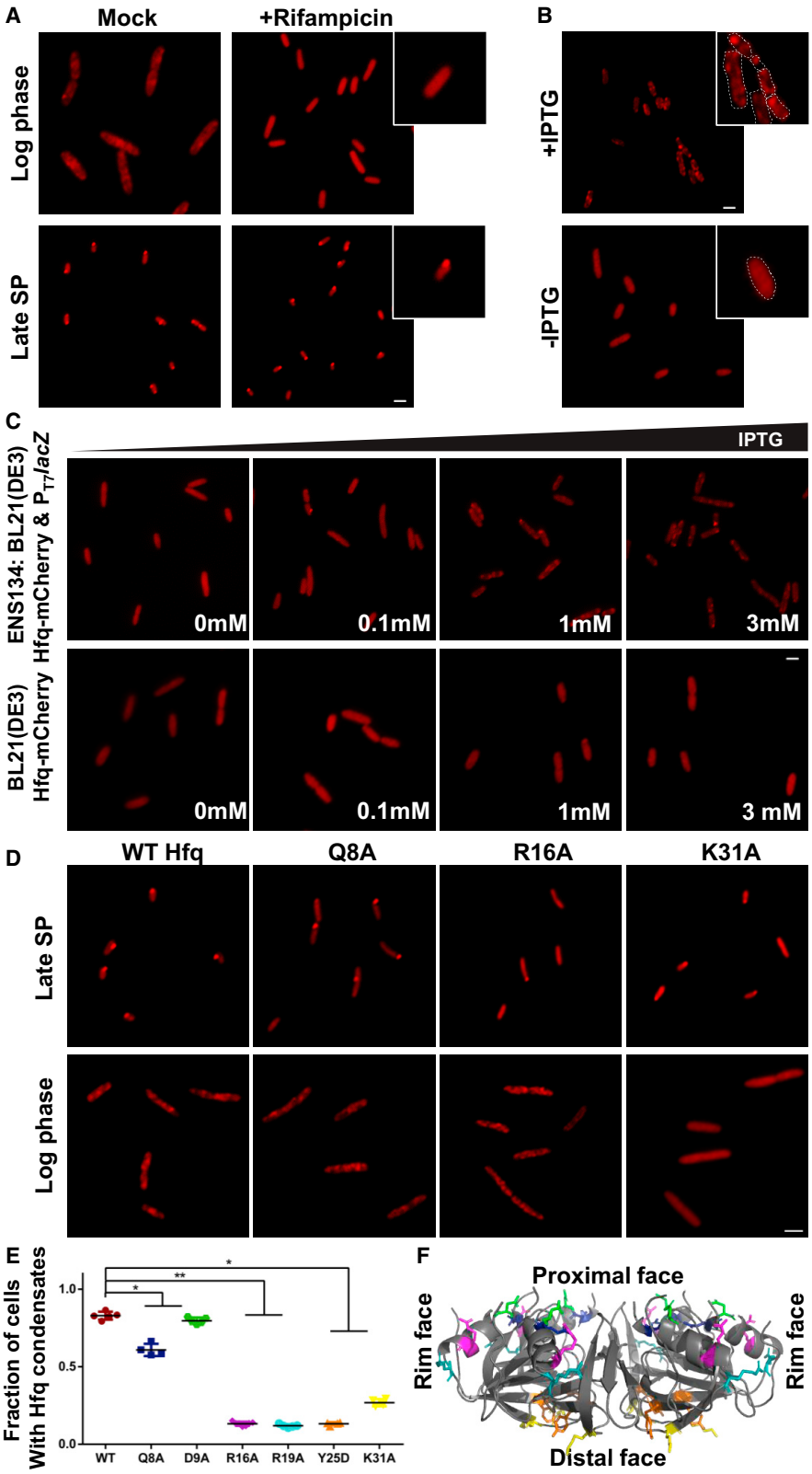

(legend on next page)

poly(A) RNA. An increase in the rate of droplet formation in a poly(A) concentration-dependent manner has been observed (Figure 2C). An increase in droplet formation was observed also in the presence of poly(U), albeit to a lower extent (Figure S10B). These results suggest that RNA facilitates Hfq phase separation and raise the possibility that RNA is required for phase separation of Hfq in the cell.

Next, we examined the ability of known Hfq RNA interactors to co-localize with Hfq droplets. Both SgrS sRNA and *ptsG* mRNA, fluorescently labeled while *in vitro* transcribed, were observed in complete co-localization with Hfq-mCherry within the droplets (Figures 2D and 2E). No signal was observed with these labeled sRNA and mRNA in the absence of Hfq (Figures S11A and S11B, respectively). Similar co-localization was documented for Hfq and a Cy3-labeled *rpoS* probe (Figure S12A). To see if both SgrS sRNA and *ptsG* mRNA, known to anneal to each other in the presence of Hfq, can co-localize simultaneously with Hfq, we mixed purified untagged Hfq with Cy3-labeled *rpoS* and Cy5-labeled DsrA probes. The results in Figures 2F and S12B demonstrate that these sRNA and mRNA co-localize in droplets depending on the presence of Hfq. These results suggest that sRNAs, mRNAs, and sRNA-mRNA pairs are capable of phase separating with Hfq.

To investigate the involvement of RNA in Hfq condensation *in vivo*, we arrested transcription by rifampicin. Hfq condensates in exponential phase cells dispersed following rifampicin treatment (Figure 3A, right panel). Of note, the polar condensates in late SP cells (late SP, Figure 3A, lower panel) did not disperse under these conditions, once again highlighting the different sensitivity of Hfq condensates between cells in the two growth phases. These results might imply that Hfq condensates in growing cells are less condense than in quiescent cells. An alternative explanation might be that the RNAs in Hfq condensates in late SP are hardly exchanged, as transcription drastically drops in this phase and most RNAs are not synthesized.

An additional support for RNA involvement in the formation of Hfq condensates was provided by monitoring Hfq-mCherry in rifampicin-treated cells overexpressing a *lacZ*-tRNA transcriptional fusion from a T7 promoter by the T7 RNA polymerase, which is not inhibited by rifampicin.[45,46] Of note, tRNAs have been shown to bind to Hfq and to be part of the Hfq-mediated sRNA interactome.[5,10] The results in Figures 3B and 3C show that Hfq condensates formed in these cells in an inducer-dependent manner, that is, depending on the rate of T7 polymerase-mediated transcription, and in a rifampicin-independent manner. Hence, RNA plays a positive role in the process of Hfq phase separation.

To get an idea on which RNA molecules might contribute to Hfq condensate formation, we turned to a set of Hfq mutants, in which single residues have been substituted in either the proximal (Q8A and D9A), rim (R16A and R19A), or distal (Y25D and K31A) face of the homohexameric ring.[47] The ability of these mutants, which are partially impaired in their association with mRNAs or with sRNAs, to form condensates was examined. The results in Figures 3D, 3E, 3F, and S13 show that mutations in the proximal face, implicated in binding and stabilizing sRNAs, had no effect on Hfq condensate formation in both growing and in late SP cells, whereas mutations in the distal face, implicated in mRNA binding, disrupted the ability of Hfq to form condensates in both growth phases almost completely. Notably, mutations in the rim face, suggested to provide additional binding sites for both sRNA and mRNA,[47,48] reduced the ability of Hfq to form polar condensates in late SP cells significantly, but had no effect on its ability to form cytoplasmic foci in growing cells. The importance of the certain faces for the formation of Hfq condensates, both in the cytoplasm and at the poles, might imply that mRNAs, but not sRNAs, are important for Hfq phase separation. Alternatively, these results might point at the distal and rim faces of Hfq as involved in the process of Hfq phase separation.

Hfq condensate formation depends on the pole-localizer TmaR

To identify other putative constituents of the Hfq condensates and shed light on the mechanism underlying its polar relocation, we asked if proteins are involved in Hfq phase separation. Because RNase E, the major component of the RNA degradosome, is a known interactor of Hfq[49,50] and was shown to cluster at the poles with Hfq and the other degradosome components during long-term nitrogen starvation,[19] we first asked if it is involved in the process of Hfq phase separation. The results in Figure S14A show that the subcellular distribution of Hfq in late SP cells was not affected by expressing RNase E from a plasmid, nor did RNase E accumulate at the poles of these cells with Hfq. RhlB, an RNA helicase and a component of the RNA degradosome, also known to interact with Hfq, was not detected as co-localizing with the polar Hfq clusters in late SP cells either (Figure S14B). Moreover, the polar Hfq condensates in late SP

Figure 3. Phase separation of Hfq depends on its distal and rim faces and on RNA

(A) Live-cell imaging of logarithmic phage (log phase, upper panels) and nutrient-deprived (late SP, lower panels) cells not treated (mock) or treated with the transcription inhibitor rifampicin (100 μg/mL, 30 min). The inserts show enlarged cells after rifampicin treatment. Scale bar, 2 μm.

(B) Live-cell imaging of Hfq-mCherry in logarithmic phase cells expressing *lacZ*-tRNA from the T7 promoter. Expression of the T7 polymerase was induced (upper image) with 1 mM IPTG for 10 min, after which the samples were treated with rifampicin (200 μg/mL, 10 min). A control of un-induced cells is presented in the lower image. The inserts show enlarged cells. Scale bar, 2 μm.

(C) Upper panel: imaging of the cells described in (B), to which an increasing concentration of IPTG was added (thus increasing the level of *lacZ*-tRNA). Lower panel: a control experiment with cells that share a similar genetic background, but do not express T7 polymerase. Scale bar, 2 μm.

(D) The effect of point mutations in the different faces of Hfq on its ability to form condensates. Fluorescence microscopy images of late SP (upper panel) and logarithmic (log) phase (lower panel) cells expressing Hfq with mutations in its proximal (Q8A), rim (R16A), or distal (K31A) faces. Images of additional mutations with different substitutions in each face are shown in Figure S13.

(E) Quantification of the ability of Hfq to form polar condensates in late SP (upper panel in (D) and Figure S13; $n > 500$ in at least 4 fields for each mutant). Statistical analysis for the differences between samples was conducted using Mann-Whitney test. The calculated p value are *0.0159 and **0.0079.

(F) Hfq crystal structure (PDB: 3QHS) with the point mutations that were examined highlighted.

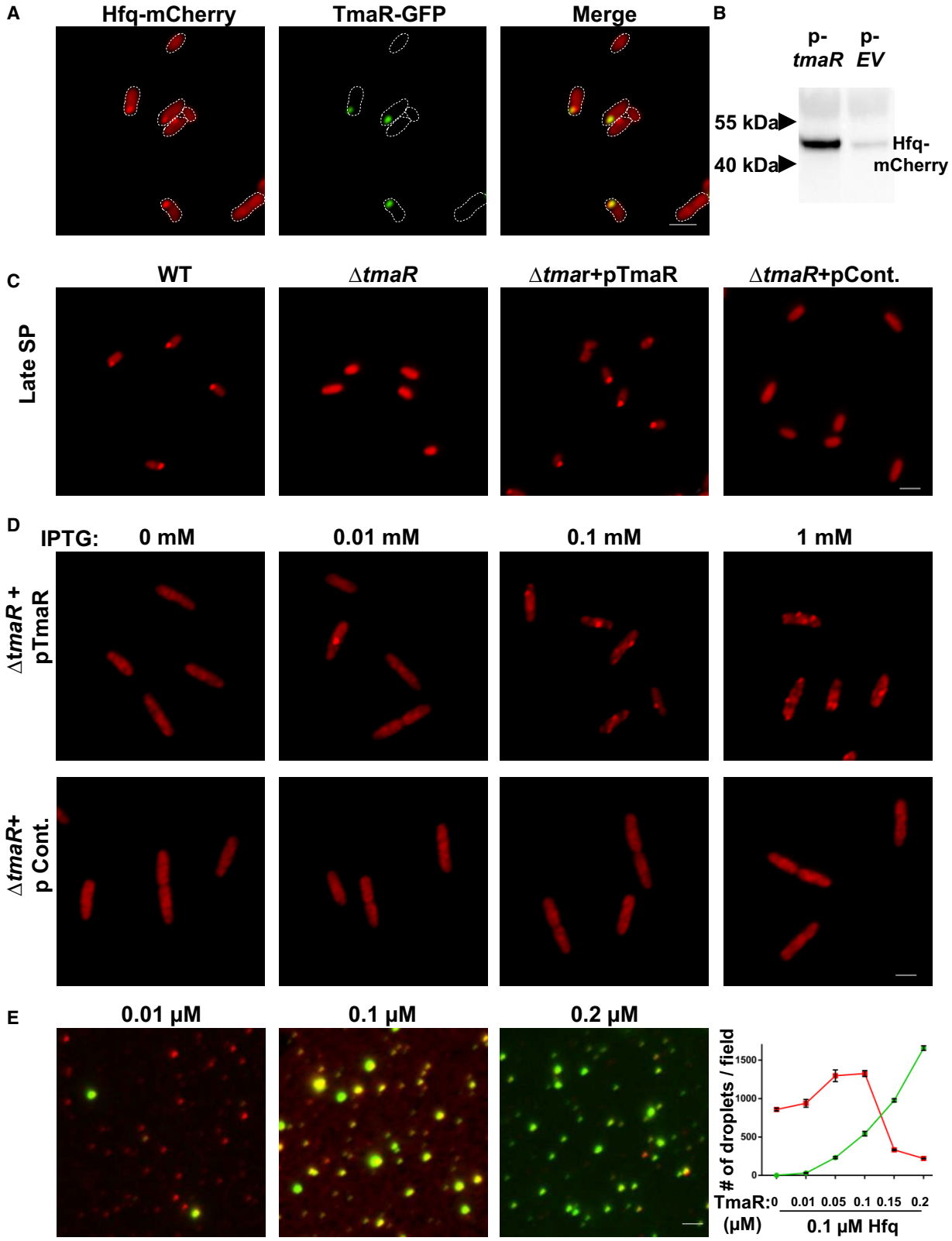

(legend on next page)

cells form in the absence RhlB (Figure S14C). Hence, the RNA degradosome does not participate in the formation of Hfq condensates. The involvement of YqjD and ElaB, which, like Hfq, localize to the poles during SP,[51,52] in Hfq condensation was also ruled out, since the pattern of Hfq distribution was not affected in cells deleted for these genes (Figure S15A).

Next, we focused on TmaR, a polar protein, recently discovered in our lab to control sugar metabolism in *E. coli* by polar sequestration and release of the general PTS protein EI[28] and shown to phase separate.[29] TmaR, previously called YeeX, was among the proteins that came up in a screen for Hfq-interacting proteins during SP.[53] Given that TmaR is polar and Hfq putative interactor during SP, we speculated that it might be involved in Hfq polar accumulation in nutrient-starved cells. We first asked if the two proteins co-localize in late SP cells, and indeed observed co-localization of Hfq-mCherry with TmaR-GFP at the poles of such cells (Figure 4A). We also observed co-localization of Hfq-mCherry with TmaR's known interactor, the EI protein, fused to GFP (Figure S15B), suggesting their mutual spatial organization. We then asked if the proteins interact by applying co-immunoprecipitation. When FLAG-tagged TmaR was pulled down from cells, Hfq-mCherry co-purified with it (Figures 4B and S16), indicating that the two co-localizing proteins interact in the cell, either directly or indirectly. Moreover, polar localization of Hfq in late SP was completely abolished in a strain lacking TmaR (Figure 4C). Expressing TmaR from a plasmid (in a *tmaR* deletion background) restored the Hfq polar condensate phenotype in nutrient-starved cells (Figure 4C). The complete dependence of Hfq polar condensate formation on TmaR was also demonstrated under high osmolarity (Figure S17A). These results indicate that Hfq relies on TmaR for its polar relocation under different stresses. Of note, no bilateral dependence for localization was observed between Hfq and TmaR, since TmaR continued to localize to the cell poles in cells deleted for *hfq* (Figure S17B). Notably, overexpression of TmaR during logarithmic growth phase, when Hfq does not cluster at the poles, resulted in an increase in Hfq condensate formation in an inducer-dependent manner, not necessarily at the poles (Figure 4D). We also assessed the impact of increasing the level of purified TmaR-GFP on Hfq *in vitro*, and the results suggest that the two proteins phase separate together (Figures 4E and S18). Of note, the Hfq-mCherry behavior in Figure S18 follows a classical phase diagram.[54] The modest increase in the number of droplets at the beginning is due to the presence of PEG. The *in vivo* and *in vitro* results of Hfq titration by TmaR further imply that TmaR plays a crucial role in Hfq condensation. Importantly, TmaR does not affect Hfq levels in the cell, nor the formation of Hfq hexamer, as the level of hexameric Hfq in Δ*tmaR* cells is comparable with that in WT cells, as shown by fractionation on a semi-native gel followed by western blot analysis and quantification (Figures 5A and S19A). Together, our results clearly indicate that not only does TmaR act as Hfq pole-localizer upon stresses and enables its polar accumulation but that it is also required for Hfq condensate formation in the cytoplasm.

To further decipher the nature of the interplay between Hfq and TmaR, we imaged Hfq-mCherry in strains expressing different TmaR variants. First, we tested whether phosphorylation of TmaR is required for Hfq phase separation. Of note, TmaR was first reported to be phosphorylated on Y79 during SP.[55] However, we have subsequently shown that, in logarithmic phase, the Y79F mutation caused only a reduction in TmaR polar clusters, whereas the Y72F mutation eliminated TmaR polar clustering.[28] Therefore, we examined Hfq localization in cells expressing TmaR mutated in each of its three tyrosines. Hfq polar accumulation was abolished only in cells expressing TmaR Y79F (Figure S19B), indicating that phosphorylation on this tyrosine is required for mediating Hfq phase separation. Next, we dissected TmaR to its domains. TmaR is composed of two alpha helices that are predicted to fold into a coiled-coil structure, both necessary for its phase separation.[29] We, therefore, tested the ability of each helix of TmaR to induce Hfq phase separation (Figure 5B, upper panel). No condensation of Hfq was observed with each helix alone, suggesting that the coiled-coil structure of TmaR, which seems important for its phase separation, is also important for its ability to induce Hfq phase separation. The effect of three-point mutations in TmaR, which impair its phase separation, on Hfq condensation was then examined. Hfq did not form condensates in cells expressing either of these TmaR mutants (Figure 5B, lower panel). Estimation of the cellular level of the above TmaR mutants and truncations, all expressed from the native *tmaR* promoter on the chromosome (Figure S19C), suggests that differences in their concentration cannot account for their different effect on Hfq phase separation. Together, these results reinforce the idea that Hfq condensation depends on TmaR phase separation.

Condensation of Hfq correlates with its ability to perform its roles in posttranscription regulation

To explore the possible biological implications of Hfq phase separation, we asked whether Hfq activity in stimulating sRNA-mRNA annealing is affected by its condensation. To this end, we performed the assay established by Ha and co-workers for

Figure 4. Hfq condensate formation depends on the pole localizer TmaR

(A) Images of Hfq-mCherry in live cells expressing TmaR-GFP and subjected to nutrient deprivation in late SP. Both fluorescent proteins were expressed from their native loci in the chromosome. Scale bar, 2 μm.

(B) Western blot analysis after immunoprecipitation (IP) of FLAG-TmaR. Hfq-mCherry was detected by anti-mCherry antibodies. Lane 1, IP of FLAG-TmaR expressed from a plasmid; lane 2, IP from cells harboring an empty vector as a control. The full membrane and bands quantification are presented in Figure S16A.

(C) Images of Hfq-mCherry in live wild-type (WT) or in Δ*tmaR* cells expressing TmaR from a plasmid (pTmaR) or containing the vector only (pCont), subjected to nutrient deprivation (late SP). Scale bar, 2 μm.

(D) Images of Hfq-mCherry in live Δ*tmaR* growing cells expressing increasing levels of TmaR from an IPTG-inducible promoter on a plasmid (pTmaR, upper panels) compared with cells with a control plasmid (pCont, lower panels). Scale bar, 2 μm.

(E) Fluorescence microscopy images showing the effect of increasing the concentration of purified TmaR-GFP on the ability of Hfq-mCherry to form droplets *in vitro* in the presence of PEG. Scale bar, 2 μm. The plot on the right shows the number of droplets formed by Hfq-mCherry (red line) and by TmaR-GFP (green line) per field. Standard errors are shown by vertical bars.

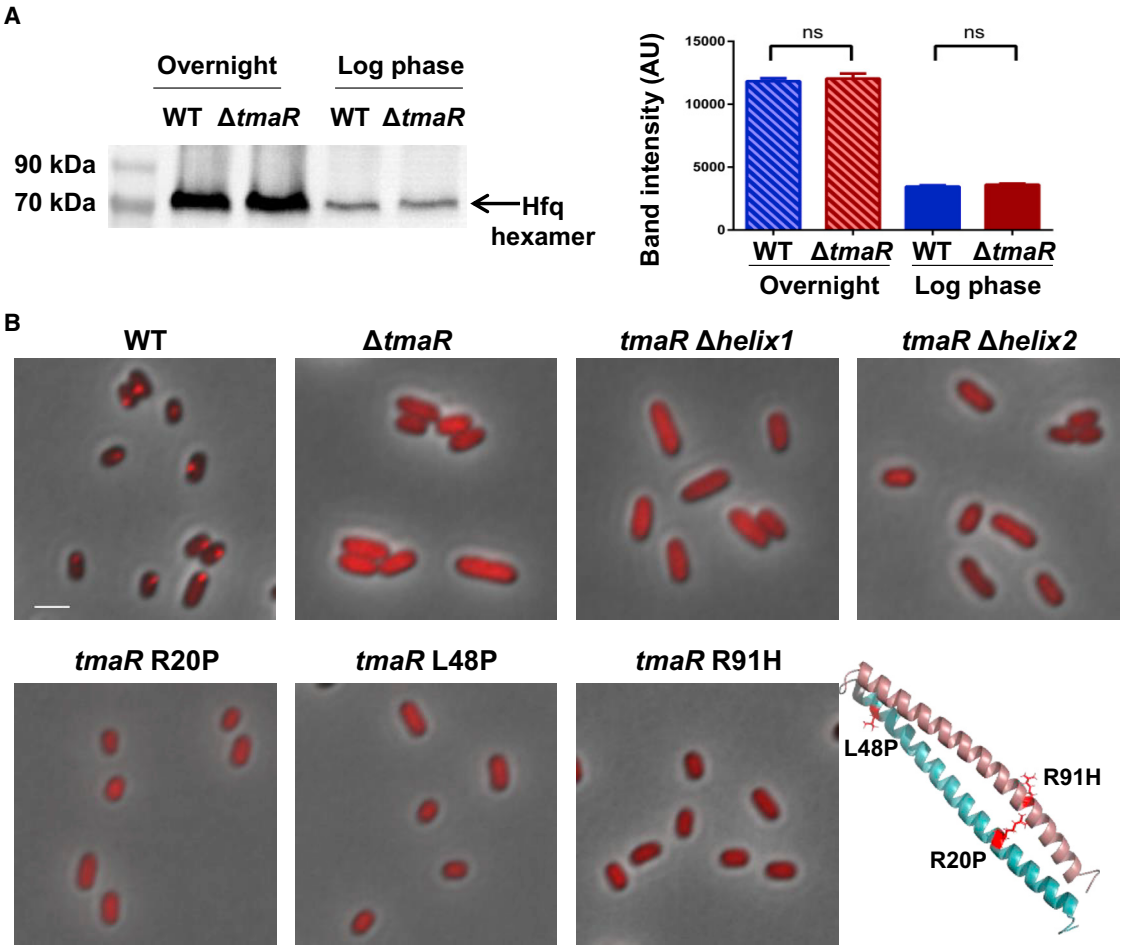

Figure 5. TmaR affects Hfq level and condensation

(A) Left panel: semi-native western blot analysis detecting Hfq-FLAG expressed from the chromosome of WT and *tmaR*-deleted cells during logarithmic growth and in late SP. The membrane was probed with anti-FLAG Ab. Right panel: comparison of Hfq-FLAG hexamer (~70 kDa) levels under both conditions examined. This experiment was repeated twice. A representative blot is presented, and the differences between the two experiments are indicated by the standard error of the mean (SEM) bars. Statistical analysis for the differences between samples was conducted using unpaired t test. ns, non-significant.

(B) Upper panel: live-cell images showing Hfq-mCherry in cells expressing WT TmaR or truncated TmaR proteins lacking the first of second alpha helix, as well as in cells deleted for *tmaR*. Scale bar, 2 μm. Lower panel: live-cell images showing Hfq-mCherry in cells expressing TmaR variants, each harboring the indicated point mutation. The mutated residues are in red in the TmaR 3D model shown on the right. Helix 1 is colored cyan and helix 2 pink.

detecting the Hfq-driven annealing of DsrA sRNA to *rpoS* mRNA, end labeled with Cys5 and Cys3, respectively (see illustration on the left in Figure 6A), by electromobility shift assay.[56] The results (Figure 6A, gels in the middle and graph on the right, and Figure S20) show that Hfq-mediated DsrA-*rpoS* annealing is dramatically reduced upon addition of hexanediol, suggesting that the activity of Hfq as an sRNA-mRNA matchmaker depends on Hfq physical state.

To further explore the implications of Hfq condensation on its chaperoning roles, we took advantage of the fact that Hfq does not undergo this process in Δ*tmaR* cells. We therefore monitored the level of various mRNAs before and during high osmolarity in WT and Δ*tmaR* cells. The results show that, except for the SP-specific *rpoS* mRNA, the level of all other mRNAs, most of them known to be involved in the applied stress, was different in cells containing Hfq condensates (WT) compared with cells lacking them (Δ*tmaR*) upon stress, and in most cases also with time in the absence of stress (Figure 6B). The results in Figure S21A show that the expression level of these transcripts was not affected by *tmaR* deletion. Hence, the process of Hfq condensation has no impact on transcription but seems important for the roles of Hfq as an mRNA chaperone at the post-transcriptional level.

To test the effect of Hfq condensation on sRNAs, we measured the level of several sRNAs, which are associated with osmotic stress, before and during high osmolarity in minicells, which package the polar content,[57] originating from WT and Δ*tmaR* cells, the latter lacking Hfq polar condensates. The sRNAs chosen were among the top ones in the list of sRNAs previously shown by us to be significantly enriched in minicells

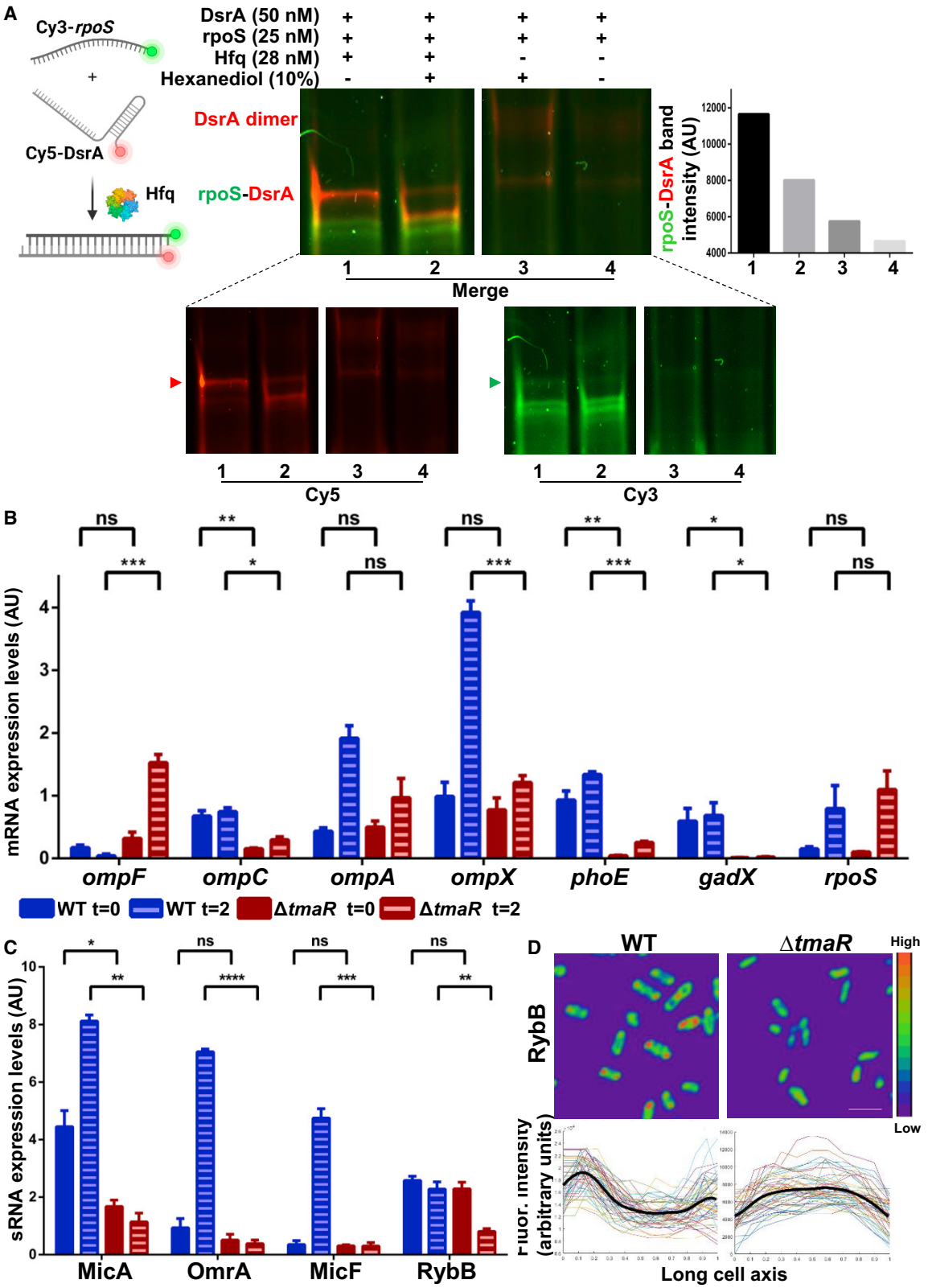

(legend on next page)

compared with whole cells (see Table S6 in Kannaiah et al.[17]) The results in Figure 6C show that the level of these sRNAs differs dramatically in Δ*tmaR* cells, which lack Hfq condensates, compared with WT, suggesting lack of stability due to the absence of their stabilizing protein. The level of three of the four sRNAs that we tested also changed over time in WT cells, probably due to the progression of the cells from exponential to SP. Hence, Hfq condensation appears important for its role as an sRNA stabilizer. Of note, the changes in mRNA and sRNA levels in Δ*tmaR* cells are not part of a global physiological defect of these cells, since their growth rate is the same of that of WT cells when recovering from both nutrient deprivation (late SP) and high osmolarity stresses (Figure S21B).

Previous results from our lab established the role of Hfq in sRNA accumulation at the poles of *E. coli* cells under high osmolarity and SP.[17] To examine the involvement of Hfq condensation on sRNA polar accumulation, we asked whether this phenomenon is abolished in cells lacking Hfq condensates, e.g., Δ*tmaR* in both stresses. Using fluorescence *in situ* hybridization, we detected the RybB and MicA sRNAs at the poles of WT cells, but not of Δ*tmaR* cells under conditions of nutrient deprivation (late SP) or high osmolarity, respectively (Figures 6D and S21C). Of note, an increase in MicA cellular level was detected in high osmolarity under the same conditions used here.[58] Hence, Hfq condensation is important for sRNA polar accumulation. Together, our results insinuate that phase separation of Hfq is important for its chaperonin and regulatory roles at the post-transcriptional level.

DISCUSSION

By and large, the evolutionary motivation for the development of membraneless organelles in bacteria are probably similar to those that led to the evolvement of membrane-bound organelles in eukaryotes, that is, the need to compartmentalize processes. Still, formation of biomolecular condensates by phase separation enables faster changes in the local concentration of macromolecules and faster exchange in the condensate composition compared with membrane-bounded organelles. This is true for all cell types but seems most suitable for unicellular organisms with short generation time, whose survival depends on the speed of their response to environmental cues. Hence, phase separation seems like an ideal organizational mechanism for bacteria. Yet, although examples for the occurrence of this phenomenon in bacteria have been recently documented, studies of phase separation in bacteria are severely lagging behind such studies in eukaryotes. Thus, whereas the roles, importance, and implications of macromolecule phase separation in eukaryotic cells are continually unraveling, similar insights are largely missing for bacteria. The main reason seems to be the small size of bacterial cells, which makes application of the methods, defined as best-practice in the field, difficult. The results presented here demonstrate that we managed to overcome these difficulties and provide high-quality proofs for phase separation-mediated condensation of Hfq, the major RNA chaperone in *E. coli*, which depends on RNA and TmaR, as well as for a strong correlation between this physical process on the ability of Hfq to carry out its roles in response to changes in the environment.

Beside its most well-characterized function as an RNA chaperone that matches sRNAs to mRNAs, Hfq plays a role in protein synthesis by binding to rRNA and tRNA and additional roles, as suggested by its binding to DNA and the pleiotropic effects caused by its deletion.[11] It is possible that condensation of TmaR-mediated Hfq is important also for these other roles. Still, the important task of Hfq condensates might be to safekeep a certain fraction of Hfq in the cell for regulating mRNA fate and making it unavailable for interaction with DNA. This notion is supported by the fact that the level of Hfq in WT *E. coli* cells (~8 μM, ~5,000 hexamers per cell) is apparently not high enough for its role as an RNA chaperone, since under some conditions it becomes limiting for RNA binding.[42] This might be explained by the fact that the level of Hfq available for binding to mRNA is much lower than measured, due to its engagement with its other substrates—DNA, tRNAs, and rRNAs.[11] Whatever the reason might be, it explains both the need for forming condensates with higher Hfq concentration in the cytoplasm and for forming bigger condensates under certain stress conditions.

Notably, not only do the cytoplasmic and polar assemblies differ in size, but they also differ in the degree of condensation of Hfq, as evidenced by their different sensitivity to hexanediol, which indicates that the cytoplasmic condensates are less condensed than the polar ones. Hence, it might very well be

Figure 6. Condensation of Hfq is important for its posttranscriptional activities

(A) An electromobility shift assay (EMSA) confirms that the DsrA-*rpoS* annealing reaction, mediated by Hfq, is impaired by hexanediol. Left panel: a schematic representation of the fluorescently labeled DsrA and *rpoS* probes and their annealing is presented. Middle panel: the EMSA results: lane 1, Cy3-*rpoS* (50 nM) and Cy5-DsrA (100 nM) incubated with Hfq (28 nM) for 15 min; lane 2, the same as lane 1, but incubation was in the presence of hexanediol (10%); lanes 3 and 4, Cy3-*rpoS* and Cy5-DsrA incubated without Hfq in the presence and absence of hexanediol, respectively. Images the split Cy5 and Cy3 channels are shown below the merged image. See the full gel in Figure S20. Right panel: the amount of RNA in the annealed form (rpoS-DsrA band) was quantified and plotted.

(B) Bar plot showing mRNA levels in WT (blue) and in Δ*tmaR* (red) cells, before (t = 0) and after 2 h (t = 2) exposure to high osmolarity stress. RNA was extracted from both strains, and the mRNAs indicated at the bottom were amplified by qPCR at the indicated time points. The color key is presented beneath the columns chart. Statistical analysis for the differences between samples was conducted using unpaired t test. The calculated p value are * ≤0.0461, ** ≤0.0044, *** ≤ 0.0008; ns, non-significant.

(C) Bar plot showing sRNA levels at the poles of WT (blue) and Δ*tmaR* (red) cells, before (t = 0) and 2 h (t = 2) after exposure to high osmolarity stress. RNA was extracted from minicells, which package the polar content, generated by both strains, and the sRNAs indicated at the bottom were amplified by qPCR at the indicated time points. The color key is shown above the columns chart and is common to Figure 6B. Statistical analysis for the differences between samples was conducted using unpaired t test. The calculated p value are *0.0443, **≤0.0053, ***0.0006, ****<0.0001; ns, non-significant.

(D) Upper panels: fluorescence *in situ* hybridization images of RybB sRNA in Δ*tmaR* (right) and WT (left) nutrient-starved cells. The fluorescence intensity key is presented by a heatmap on the right. Lower panels: fluorescence intensity profiles plotted along the long cell axis after normalizing to cell length (n = 50 of each strain). Scale bar, 2 μm.

that the cytoplasmic and polar Hfq condensates differ also in their content. The identity of the polar and non-polar constituents, besides RNA and TmaR, that are required for forming the two types of Hfq condensates is a subject for future research. The facing-out residues in the distal and rim faces of the Hfq hexamer, shown here to be required for Hfq phase separation, might be engaged in interaction with the other condensate components.

Relocation of the bigger Hfq clusters to the poles could have been explained by the space available in these domains due to nucleoid occlusion, but we show here that condensing the chromosome by the addition of chloramphenicol did not affect the formation of Hfq polar foci. Also, the reduction in *E. coli* cell size, observed in late SP, cannot account for the formation of polar Hfq condensates due to an increase in Hfq concentration, since polar Hfq condensates are also formed in cells that do not shrink as much, such as cells that are osmotically stressed. Moreover, cells harboring various Hfq mutants that impair their function look similar in size to cells at high osmolarity, but still no polar condensates are formed (e.g., Figure 3D). Thus, small size is apparently not the cause for polar Hfq localization.

Of note, data to date suggest that the cytoplasm of unstressed *E. coli* is actually a viscoelastic material (Bhat et al.[59] and references therein), and that the cytoplasm of stressed bacteria displays properties characteristic of glass or hardened gel.[60] The type of analyses reported here cannot determine the exact material state—liquid or gel—of Hfq in the condensates and in the coexisting dilute phase.

Condensation of RBPs is expected to have spatial implications on the RNAs they bind. Indeed, phase separation of RNPs was suggested to assist in RNA localization in eukaryotes.[43] Then again, RNA may assist in phase separation of proteins, mainly, although not only, due to its ability to serve as a scaffold molecule for several proteins to enable their condensation by heterotypic interactions.[27,61] In this respect, Hfq hexamers were suggested to associate by RNA-RNA interaction via a motif that is present in a subset of sRNAs.[62] The findings reported here, showing that RNAs both co-localize with Hfq condensates and are required for condensation of purified Hfq and in the cell, support the notion that Hfq requires RNAs, since it phase separates with them by heterotypic interactions. Our previous[17] and current results show that localization and stability of sRNAs in particular, but also of mRNAs, depend on Hfq localization and condensation, but the question whether it is Hfq or the RNAs that initiate the process is of the chicken and egg causality dilemma type. Unless TmaR serve as a scaffold for Hfq phase separation, RNA may very well serve as its scaffold, since Hfq is evidently a client in this process.

Since Hfq is an Sm-like protein, conserved throughout evolution, and sRNAs play key regulatory roles in eukaryotes as well, our findings are relevant also for higher cells. An example for such relevance is our recent study, which shows accumulation of numerous sRNAs in the poles as part of the plan of *E. coli* cells for coping with stresses,[63] which corresponds with a study just published that shows co-localization of hundreds of non-coding RNAs in higher eukaryotic cells within spatial compartments in the nucleus, which recruit RNA and protein regulators, thus controlling processes underpinning gene expression.[64]

The resources that bacteria invest to specifically localize and condense macromolecules during stress conditions, when recourses are scarce, highlight the importance of subcellular organization for their survival. The evolutionary driving force for the development of organizational mechanisms, such as phase separation, might be the need to sequester macromolecules for keeping them inactive or secluded under certain conditions. Alternatively, the gain might be in the creation of a favorable environment for the activation of macromolecules and processes. In both cases, time is an important factor when adapting to a new environment, and the quick changes in macromolecule activity offered by membraneless organelles is an advantage.

Limitations of the study

We show that both RNA and TmaR are required for Hfq condensation, but we did not address the question how the stoichiometry between the three components impacts condensate formation, nor their relative importance of these components for Hfq condensation. Moreover, although we show that Hfq phase separates by heterotypic interactions with both RNA and TmaR, we cannot exclude the existence of a blend of homotypic and heterotypic interactions in the condensates. In addition, we did not determine the exact material state of Hfq condensates and the coexisting dilute phase. Therefore, we refrained from using the term liquid-liquid phase separation and preferred to use the term phase separation. The linkage between the material state of Hfq and its different activities as an RNA chaperon is based mainly on correlative evidence, awaiting future development of methodologies for proving direct dependence. Finally, we cannot rule out that nano-droplets of Hfq assembled but remained undetected at the resolution of our analysis in some of the experiments.

STAR★METHODS

Detailed methods are provided in the online version of this paper and include the following:

- KEY RESOURCES TABLE
- RESOURCE AVAILABILITY
  - Lead contact
  - Materials availability
  - Data and code availability
- EXPERIMENTAL MODEL AND SUBJECT DETAILS
  - Growth conditions
- METHOD DETAILS
  - Strain construction
  - Plasmid construction
  - Fluorescent microscopy
  - Immunostaining
  - Fluorescence recovery after photo bleaching (FRAP)
  - Protein purification
  - *In vitro* liquid-liquid phase separation assays
  - *In vitro* transcription and labeling
  - Co-immunoprecipitation for detecting Hfq-TmaR interaction
  - Fluorescence *in situ* hybridization (FISH)
  - Minicells purification

- RT-qPCR
- GFP reporter assay
- Growth test
- Western blot analysis
- Semi-native Western blot analysis
- Promoter GFP assay
- Electro-mobility shift assay (EMSA)

● QUANTIFICATION AND STATISTICAL ANALYSIS

SUPPLEMENTAL INFORMATION

Supplemental information can be found online at https://doi.org/10.1016/j.celrep.2022.111881.

ACKNOWLEDGMENTS

We acknowledge Susan Gottesman for the gift of strains with Hfq single amino acid substitutions, Agamemnon Carpusis for the gift of the ENS134 strain and the pVK207 plasmid, Jörg Vogel for the gift of plasmids expressing sRNAs and mRNAs fused to GFP for the translational control assays, and Uri Alon for the gift of plasmids expressing GFP from the promoters of *ompA*, *ompC*, *ompX*, *gadX*, and *rpoS* genes. We appreciate fruitful discussions with members of the O.A.-C. lab, Hanah Margalit, Liron Argaman, and Maya Elgrably-Weiss. This research was supported by the Israel Science Foundation (ISF) founded by the Israel Academy of Sciences and Humanities (1274/19). O.G. is funded by a PhD fellowship from the Israel Ministry of Science and Technology (19400201).

AUTHOR CONTRIBUTIONS

O.A.-C. and O.G. designed of the study. O.G. and A.N.-S. generated the strains and plasmids. O.G. conducted the experiments and analyzed the data. O.G., T.S., A.N.-S., and O.A.-C. contributed to data interpretation. O.A.-C. and O.G. wrote the manuscript. O.A.-C. supervised the study, provided advice, and contributed to experimental design.

DECLARATION OF INTERESTS

The authors declare no competing interests.

Received: December 26, 2021
Revised: November 25, 2022
Accepted: December 3, 2022
Published: December 27, 2022

REFERENCES

1. Bacterial Stress Responses. ASM Press (ASM Press, 2010). https://doi.org/10.1128/9781555816841.
2. Hör, J., Matera, G., Vogel, J., Gottesman, S., and Storz, G. (2020). Trans-Acting small RNAs and their effects on gene expression in Escherichia coli and Salmonella enterica. EcoSal Plus *9*.
3. Holmqvist, E., and Wagner, E.G.H. (2017). Impact of bacterial sRNAs in stress responses. Biochem. Soc. Trans. *45*, 1203–1212.
4. Storz, G., Vogel, J., and Wassarman, K.M. (2011). Regulation by small RNAs in bacteria: expanding frontiers. Mol. Cell *43*, 880–891.
5. Melamed, S., Peer, A., Faigenbaum-Romm, R., Gatt, Y.E., Reiss, N., Bar, A., Altuvia, Y., Argaman, L., and Margalit, H. (2016). Global mapping of small RNA-target interactions in bacteria. Mol. Cell *63*, 884–897.
6. Holmqvist, E., Li, L., Bischler, T., Barquist, L., and Vogel, J. (2018). Global maps of ProQ binding in vivo reveal target recognition via RNA structure and stability control at mRNA 3′ ends. Mol. Cell *70*, 971–982.e6.
7. Quendera, A.P., Seixas, A.F., Dos Santos, R.F., Santos, I., Silva, J.P.N., Arraiano, C.M., and Andrade, J.M. (2020). RNA-binding proteins driving the regulatory activity of small non-coding RNAs in bacteria. Front. Mol. Biosci. *7*, 1–9.
8. Vogel, J., and Luisi, B.F. (2011). Hfq and its constellation of RNA. Nat. Rev. Microbiol. *9*, 578–589.
9. Schumacher, M.A., Pearson, R.F., Møller, T., Valentin-Hansen, P., and Brennan, R.G. (2002). Structures of the pleiotropic translational regulator Hfq and an Hfq-RNA complex: a bacterial Sm-like protein. EMBO J. *21*, 3546–3556.
10. Schu, D.J., Zhang, A., Gottesman, S., and Storz, G. (2015). Alternative Hfq-sRNA interaction modes dictate alternative mRNA recognition. EMBO J. *34*, 2557–2573.
11. dos Santos, R.F., Arraiano, C.M., and Andrade, J.M. (2019). New molecular interactions broaden the functions of the RNA chaperone Hfq. Curr. Genet. *65*, 1313–1319.
12. Muffler, A., Traulsen, D.D., Fischer, D., Lange, R., and Hengge-Aronis, R. (1997). The RNA-binding protein HF-I plays a global regulatory role which is largely, but not exclusively, due to its role in expression of the σ(S) subunit of RNA polymerase in Escherichia coli. J. Bacteriol. *179*, 297–300.
13. Monteiro, C., Papenfort, K., Hentrich, K., Ahmad, I., Guyon, S.L., Reimann, R., Grantcharova, N., and Römling, U. (2012). Hfq and Hfq-dependent small RNAs are major contributors to multicellular development in Salmonella enterica serovar typhimurium. RNA Biol. *9*, 489–502.
14. Malabirade, A., Morgado-Brajones, J., Trépout, S., Wien, F., Marquez, I., Seguin, J., Marco, S., Velez, M., and Arluison, V. (2017). Membrane association of the bacterial riboregulator Hfq and functional perspectives. Sci. Rep. *7*, 1–12.
15. Taghbalout, A., Yang, Q., and Arluison, V. (2014). The Escherichia coli RNA processing and degradation machinery is compartmentalized within an organized cellular network. Biochem. J. *458*, 11–22.
16. Fortas, E., Piccirilli, F., Malabirade, A., Militello, V., Trépout, S., Marco, S., Taghbalout, A., and Arluison, V. (2015). New insight into the structure and function of Hfq C-terminus. Biosci. Rep. *35*, 1–9.
17. Kannaiah, S., Livny, J., and Amster-Choder, O. (2019). Spatiotemporal organization of the E. coli transcriptome: translation independence and engagement in regulation. Mol. Cell *76*, 574–589.e7.
18. McQuail, J., Switzer, A., Burchell, L., and Wigneshweraraj, S. (2020). The RNA-binding protein Hfq assembles into foci-like structures in nitrogen starved Escherichia coli. J. Biol. Chem. *295*, 12355–12367.
19. McQuail, J., Carpousis, A.J., and Wigneshweraraj, S. (2021). The association between Hfq and RNase E in long-term nitrogen-starved Escherichia coli. Mol. Microbiol. *117*, 54–66. https://doi.org/10.1111/mmi.14782.
20. Lin, Y., Protter, D.S.W., Rosen, M.K., and Parker, R. (2015). Formation and maturation of phase-separated liquid droplets by RNA-binding proteins. Mol. Cell *60*, 208–219.
21. Al-Husini, N., Tomares, D.T., Bitar, O., Childers, W.S., and Schrader, J.M. (2018). α-Proteobacterial RNA degradosomes assemble liquid-liquid phase-separated RNP bodies. Mol. Cell *71*, 1027–1039.e14.
22. Shin, Y., and Brangwynne, C.P. (2017). Liquid phase condensation in cell physiology and disease. Science *357*.
23. Azaldegui, C.A., Vecchiarelli, A.G., and Biteen, J.S. (2020). The emergence of phase separation as an organizing principle in bacteria. Biophys. J. *121*, 1123–1138. https://doi.org/10.1016/j.bpj.2020.09.023.
24. Cohan, M.C., and Pappu, R.V. (2020). Making the case for disordered proteins and biomolecular condensates in bacteria. Trends Biochem. Sci. *45*, 668–680.
25. Lasker, K., von Diezmann, L., Zhou, X., Ahrens, D.G., Mann, T.H., Moerner, W.E., and Shapiro, L. (2020). Selective sequestration of signalling proteins in a membraneless organelle reinforces the spatial regulation of asymmetry in Caulobacter crescentus. Nat. Microbiol. *5*, 418–429.
26. Monterroso, B., Zorrilla, S., Sobrinos-Sanguino, M., Robles-Ramos, M.A., López-Álvarez, M., Margolin, W., Keating, C.D., and Rivas, G. (2019). Bacterial FtsZ protein forms phase-separated condensates with its nucleoid-associated inhibitor SlmA. EMBO Rep. *20*, 1–13.

27. Roden, C., and Gladfelter, A.S. (2020). RNA contributions to the form and function of biomolecular condensates. Nat. Rev. Mol. Cell Biol. *22*, 183–195. https://doi.org/10.1038/s41580-020-0264-6.

28. Szoke, T., Albocher, N., Govindarajan, S., Nussbaum-Shochat, A., and Amster-Choder, O. (2021). Tyrosine phosphorylation-dependent localization of TmaR that controls activity of a major bacterial sugar regulator by polar sequestration. Proc. Natl. Acad. Sci. USA *118*.

29. Szoke, T., Albocher, N., Goldberger, O., Barsheshet, M., Nussbaum-Shochat, A., Wiener, R., Schuldiner, M., and Amster-Choder, O. (2022). Regulation of major bacterial survival strategies by transcript sequestration in a membraneless organelle. Preprint at bioRxiv. https://doi.org/10.1101/2022.01.06.475198.

30. Sun, Y., and Vanderpool, C.K. (2013). Physiological consequences of multiple-target regulation by the small RNA SgrS in escherichia coli. J. Bacteriol. *195*, 4804–4815.

31. Richards, J., and Belasco, J.G. (2019). Obstacles to scanning by RNase E govern bacterial mRNA lifetimes by hindering access to distal cleavage sites. Mol. Cell *74*, 284–295.e5.

32. Morita, T., Maki, K., and Aiba, H. (2005). RNase E-based ribonucleoprotein complexes: mechanical basis of mRNA destabilization mediated by bacterial noncoding RNAs. Genes Dev. *19*, 2176–2186.

33. Urban, J.H., and Vogel, J. (2007). Translational control and target recognition by Escherichia coli small RNAs in vivo. Nucleic Acids Res. *35*, 1018–1037.

34. Govers, S.K., Mortier, J., Adam, A., and Aertsen, A. (2018). Protein aggregates encode epigenetic memory of stressful encounters in individual Escherichia coli cells. PLoS Biol. *16*.

35. Alberti, S., Gladfelter, A., and Mittag, T. (2019). Considerations and challenges in studying liquid-liquid phase separation and biomolecular condensates. Cell *176*, 419–434.

36. Chong, S., Dugast-Darzacq, C., Liu, Z., Dong, P., Dailey, G.M., Cattoglio, C., Heckert, A., Banala, S., Lavis, L., Darzacq, X., and Tjian, R. (2018). Imaging dynamic and selective low-complexity domain interactions that control gene transcription. Science *361*.

37. Lancaster, A.K., Nutter-Upham, A., Lindquist, S., and King, O.D. (2014). PLAAC: a web and command-line application to identify proteins with prion-like amino acid composition. Bioinformatics *30*, 2501–2502.

38. Toombs, J.A., Petri, M., Paul, K.R., Kan, G.Y., Ben-Hur, A., and Ross, E.D. (2012). De novo design of synthetic prion domains. Proc. Natl. Acad. Sci. USA *109*, 6519–6524.

39. Wen, B., Wang, W., Zhang, J., Gong, Q., Shi, Y., Wu, J., and Zhang, Z. (2017). Structural and dynamic properties of the C-terminal region of the: Escherichia coli RNA chaperone Hfq: integrative experimental and computational studies. Phys. Chem. Chem. Phys. *19*, 21152–21164.

40. Beaufay, F., Amemiya, H.M., Guan, J., Basalla, J., Meinen, B.A., Chen, Z., Mitra, R., Bardwell, J.C.A., Biteen, J.S., Vecchiarelli, A.G., et al. (2021). Polyphosphate drives bacterial heterochromatin formation. Sci. Adv. *7*, 233.

41. Hatos, A., Tosatto, S.C.E., Vendruscolo, M., and Fuxreiter, M. (2022). FuzDrop on AlphaFold: visualizing the sequence-dependent propensity of liquid-liquid phase separation and aggregation of proteins. Nucleic Acids Res. *50*, W337–W344.

42. Argaman, L., Elgrably-Weiss, M., Hershko, T., Vogel, J., and Altuvia, S. (2012). RelA protein stimulates the activity of RyhB small RNA by acting on RNA-binding protein Hfq. Proc. Natl. Acad. Sci. USA *109*, 4621–4626.

43. Langdon, E.M., and Gladfelter, A.S. (2018). A new lens for RNA localization: liquid-liquid phase separation. Annu. Rev. Microbiol. *72*, 255–271.

44. Rhine, K., Vidaurre, V., and Myong, S. (2020). RNA droplets. Annu. Rev. Biophys. *49*, 247–265.

45. Lopez, P.J., Iost, I., and Dreyfus, M. (1994). The use of a tRNA as a transcriptional reporter: the '17 late promoter is extremely efficient in escherichia coil but its transcripts are poorly expressed. Nucleic Acids Res. *22*, 2434.

46. Strahl, H., Turlan, C., Khalid, S., Bond, P.J., Kebalo, J.M., Peyron, P., Poljak, L., Bouvier, M., Hamoen, L., Luisi, B.F., and Carpousis, A.J. (2015). Membrane recognition and dynamics of the RNA degradosome. PLoS Genet. *11*, 1–23.

47. Zhang, A., Schu, D.J., Tjaden, B.C., Storz, G., and Gottesman, S. (2013). Mutations in interaction surfaces differentially impact E. coli Hfq association with small RNAs and their mRNA targets. J. Mol. Biol. *425*, 3678–3697.

48. Sauer, E., Schmidt, S., and Weichenrieder, O. (2012). Small RNA binding to the lateral surface of Hfq hexamers and structural rearrangements upon mRNA target recognition. Proc. Natl. Acad. Sci. USA *109*, 9396–9401.

49. Bruce, H.A., Du, D., Matak-Vinkovic, D., Bandyra, K.J., Broadhurst, R.W., Martin, E., Sobott, F., Shkumatov, A.V., and Luisi, B.F. (2018). Analysis of the natively unstructured RNA/protein-recognition core in the Escherichia coli RNA degradosome and its interactions with regulatory RNA/Hfq complexes. Nucleic Acids Res. *46*, 387–402.

50. Carabetta, V.J., Silhavy, T.J., and Cristea, I.M. (2010). The response regulator SprE (RssB) is required for maintaining poly(A) polymerase I-degradosome association during stationary phase. J. Bacteriol. *192*, 3713–3721.

51. Li, G., and Young, K.D. (2012). Isolation and identification of new inner membrane-associated proteins that localize to cell poles in Escherichia coli. Mol. Microbiol. *84*, 276–295.

52. Guo, Y., Liu, X., Li, B., Yao, J., Wood, T.K., and Wang, X. (2017). Tail-anchored inner membrane protein ElaB increases resistance to stress while reducing persistence in Escherichia coli. J. Bacteriol. *199*.

53. Caillet, J., Baron, B., Boni, I.V., Caillet-Saguy, C., and Hajnsdorf, E. (2019). Identification of protein-protein and ribonucleoprotein complexes containing Hfq. Sci. Rep. *9*, 1–12.

54. Gao, Z., Zhang, W., Chang, R., Zhang, S., Yang, G., and Zhao, G. (2021). Liquid-liquid phase separation: unraveling the enigma of biomolecular condensates in microbial cells. Front. Microbiol. *12*.

55. Soares, N.C., Spät, P., Krug, K., and MacEk, B. (2013). Global dynamics of the Escherichia coli proteome and phosphoproteome during growth in minimal medium. J. Proteome Res. *12*, 2611–2621.

56. Arluison, V., Hohng, S., Roy, R., Pellegrini, O., Régnier, P., and Ha, T. (2007). Spectroscopic observation of RNA chaperone activities of Hfq in post-transcriptional regulation by a small non-coding RNA. Nucleic Acids Res. *35*, 999–1006.

57. Lai, E.M., Nair, U., Phadke, N.D., and Maddock, J.R. (2004). Proteomic screening and identification of differentially distributed membrane proteins in Escherichia coli. Mol. Microbiol. *52*, 1029–1044.

58. Udekwu, K.I., and Wagner, E.G.H. (2007). Sigma E controls biogenesis of the antisense RNA MicA. Nucleic Acids Res. *35*, 1279–1288.

59. Bhat, S., Jun, D., Paul, B.C., and Dahms, T.E.S. (2012). Viscoelasticity in biological systems: a special Focus on microbes. In Viscoelasticity - From Theory to Biological Applications (IntechOpen). https://doi.org/10.5772/49980.

60. Parry, B.R., Surovtsev, I.V., Cabeen, M.T., O'Hern, C.S., Dufresne, E.R., and Jacobs-Wagner, C. (2014). The bacterial cytoplasm has glass-like properties and is fluidized by metabolic activity. Cell *156*, 183–194.

61. Poudyal, R.R., Sieg, J.P., Portz, B., Keating, C.D., and Bevilacqua, P.C. (2021). RNA sequence and structure control assembly and function of RNA condensates. RNA *41*, 1589–1601. https://doi.org/10.1261/rna.078875.121.

62. Schulz, E.C., Seiler, M., Zuliani, C., Voigt, F., Rybin, V., Pogenberg, V., Mücke, N., Wilmanns, M., Gibson, T.J., and Barabas, O. (2017). Intermolecular base stacking mediates RNA-RNA interaction in a crystal structure of the RNA chaperone Hfq. Sci. Rep. *7*, 1–15.

63. Goldberger, O., Livny, J., Bhattacharyya, R., and Amster-Choder, O. (2021). Wisdom of the crowds: a suggested polygenic plan for small-RNA-mediated regulation in bacteria. iScience *24*.

64. Quinodoz, S.A., Jachowicz, J.W., Bhat, P., Ollikainen, N., Banerjee, A.K., Goronzy, I.N., Blanco, M.R., Chovanec, P., Chow, A., Markaki, Y., et al.

(2021). RNA promotes the formation of spatial compartments in the nucleus. Cell *184*, 5775–5790.e30.

65. Baba, T., Ara, T., Hasegawa, M., Takai, Y., Okumura, Y., Baba, M., Datsenko, K.A., Tomita, M., Wanner, B.L., and Mori, H. (2006). Construction of Escherichia coli K-12 in-frame, single-gene knockout mutants: the Keio collection. Mol. Syst. Biol. *2*.

66. Li, X., Thomason, L.C., Sawitzke, J.A., Costantino, N., and Court, D.L. (2013). Positive and negative selection using the tetA-sacB cassette : recombineering and P1 transduction in Escherichia coli. Nucleic Acids Res. *41*, e204.

67. Gibson, D.G., Young, L., Chuang, R.Y., Venter, J.C., Hutchison, C.A., 3rd, and Smith, H.O. (2009). Enzymatic assembly of DNA molecules up to several hundred kilobases. Nat. Methods *6*, 343–345.

68. Basu, P., Elgrably-Weiss, M., Hassouna, F., Kumar, M., Wiener, R., and Altuvia, S. (2021). RNA binding of Hfq monomers promotes RelA-mediated hexamerization in a limiting Hfq environment. Nat. Commun. *12*.

69. Nevo-Dinur, K., Nussbaum-Shochat, A., Ben-Yehuda, S., and Amster-Choder, O. (2011). Translation-independent localization of mRNA in E. coli. Science *331*, 1081–1084.

STAR★METHODS

KEY RESOURCES TABLE

REAGENT or RESOURCE	SOURCE	IDENTIFIER
Antibodies		
The FLAG Tag Antibody, mAb, Mouse	GenScript	Cat#A00187
Alexa Fluor 594, Anti-Mouse IgG (H + L)	Invitrogen	Cat#A11005
Anti mCherry	Abcam	Cat#ab167453
Anti GroEL	Abcam	Cat#ab90522
Chemicals, peptides, and recombinant proteins		
Ampicillin	AppliChem Panreac	Cat#A0389
Chloramphenicol	Sigma-Aldrich	Cat #C0378
Kanamycin sulfate	Biological Industries	Cat#25389-94-0
Rifampicin	Goldbio	Cat#R-120-5
Sucrose	Sigma-Aldrich	Cat#S0389
TriReagent Solution	Sigma-Aldrich	Cat#T9424
DMSO	Sigma Aldrich	Cat#D2438
Ultra-pure water, RNase- and DNase-free	Biological Industries	Cat#01-866-1A
InstantBlue® Protein Stain	Expedeon	Cat#ISB1L
Ponceau S	Sigma-Aldrich	Cat#P7170
BD Difco™ M9 Minimal Salts	BD Biosciences	Cat#248510
Poly(ethylene glycol) 8000	Sigma-Aldrich	Cat#P2139
Poly(A), Polyadenylitic acid	GE Healthcare	Cat#27-4110-01
Poly(U), Polyuridylic acid potassium salt	Sigma-Aldrich	Cat#P9528
Ni-NTA beads	Thermo Fisher Scientific	Cat#88222
HEPES	Sigma-Aldrich	Cat#H3375
Hexanediol	Sigma-Aldrich	Cat#240117
DAPI (4-,6-diamidino-2-phenylindole)	Sigma-Aldrich	Cat#D8417
Sodium lauroyl sarcosinate (Sarkosyl)	Sigma-Aldrich	Cat#L9150
Critical commercial assays		
iTaq Universal SYBER Green Supermix	Bio-Rad	Cat#1725121
Direct-zol RNA Miniprep Kit	Zymo Research	Cat#R2060
qScript cDNA Synthesis Kit	Quanta bio	Cat#95047–100
Qubit RNA HS Assay Kit	Thermo Scientific	Cat#Q32852
Turbo DNA-free Kit	Ambion	Cat#AM1907
NucleoSpin Plasmid EasyPure Kit	Machery-Nagel	Cat#740727
NucleoSpin Gel and PCR clean-up Kit	Machery-Nagel	Cat#740609
Qubit dsDNA High Sensitivity Kit	Life Technologies	Cat#Q32854
EZ-ECL	Biological Industries	Cat#20-500-120
Gravity column	Bio-Rad	Cat#732–1010
HighYield T7 AF488 RNA Labeling Kit	Jena Bioscience	Cat#RNT-101-AF488
Turbo™DNAse	Thermo Fisher	Cat# AM2238
RNA Clean & Concentrator Kits	Zymo Research	Cat# R1015
Anti-DYKDDDDK G1 Affinity Resin	GenScript	Cat# L00432
Software and algorithms		
NIS Elements Advanced Research (AR) version 4.5	Nikon	N/A
GraphPad Prism v6	GraphPad	https://www.graphpad.com/scientific-software/prism/
Image Lab v6.0.1	Bio-Rad	http://www.bio-rad.com/en-il/product/image-lab-software
R	The R Foundation	https://www.r-project.org/

RESOURCE AVAILABILITY

Lead contact

Further information and requests should be directed to the lead contact, Orna Amster-Choder (ornaam@ekmd.huji.ac.il).

Materials availability

Bacterial strains and plasmids will be made available upon request.

Data and code availability

This paper does not report new or original code.

The raw data for the manuscript is available on request from the lead contact Prof. Orna Amster-Choder (ornaam@ekmd.huji.ac.il).

Any additional information required to reanalyze the data reported in this paper is available from the lead contact upon request.

EXPERIMENTAL MODEL AND SUBJECT DETAILS

Growth conditions

Strains, plasmids, and primers used in this study are listed in Tables S1, S2 and S3. Bacterial cells were grown at 30ºC in LB medium. When appropriate, antibiotics were added at the following concentrations: kanamycin (30 μg/mL), ampicillin (200 μg/mL) and chloramphenicol (25 μg/mL). As indicated, proteins were expressed from the chromosome or plasmids induced by IPTG at the indicated concentration. Overnight cultures (grown for 16 h with aeration) were used for nutrient-deprivation experiments. To induce envelope stress, cells were grown to mid-logarithmic phase, pelleted, and resuspended in fresh LB medium containing 20% sucrose or 0.3M NaCl and further grown for the desired time. To induce oxidative stress or iron limitation, 1mM hydrogen peroxide or 0.2mM 2,20-dipyridyl were added, respectively, at mid-logarithmic phase and cells were further grown for the indicated time. Translation and transcription were arrested by the addition of 200 μg/mL of chloramphenicol for 15 min and 100 μg/mL of rifampicin for the last 30, respectively. For minimal media, M9 Minimal Salts was used according to the manufacturer's instructions and carbon sources (glucose or succinate) were added when needed. For conditioned medium, a culture of OG172 was grown in LB overnight (16 h) followed by filtration, using a 0.2 μm syringe filter to eliminate bacteria.

METHOD DETAILS

Strain construction

To construct strain OG167, which contains Hfq-mCherry-kan, Hfq-mCherry fragment was amplified from a pBAD18-Hfq-mCherry plasmid. The kanamycin cassette was amplified from pKD4 plasmid. The two amplicons were ligated by Gibson assembly. The assembled fragment was amplified by primers from the ends and introduced into MG1655 strain containing pKD46 plasmid. The verified cells were grown at 42ºC and tested for loss of pKD46. pCP20 plasmid was used to remove the kanamycin cassette resulting in the construction of the OG172 strain.

Strain OG184 which contains Hfq-mCherry and IbpA-sfGFP was constructed by P1 transduction of *IbpAmsfgfp*:*kan* from IbpA-msfGFP strain[34] to MG1655-Hfq-mCherry.

Strain OG185 (MG1655 Δhfq) with no antibiotic resistance was constructed by removing the Kan cassette from MG1655Δ*hfq*:*kan* using pCP20.

Strains OG274 (BL21(DE3) Hfq-mCherry-kan) and OG265 (ENS134 Hfq-mCherry-kan) were constructed by P1 transduction of Hfq-mCherry-Kan cassette to BL21(DE3) and ENS134, respectively.

To create strains expressing Hfq-mCherry with single point mutations (Q8A, D9A, R16A, R19A, Y25D, and K31A), the mCherry-kan fragment from strain OG167 (MG1655 Hfq-mCherry-kan) was amplified. The amplicon was transformed into an MG1655 derivative with the respective point mutations. P1 lysates were made from each strain and the corresponding Hfq-mCherry-kan fragments were transduced into wild-type MG1655.

Strain OG249, a strain that co-expresses RhlB-YFP and Hfq-mCherry was constructed by P1 transduction of wild-type Hfq-mCherry-kan fragment from strain OG165 (MG1655 Hfq-mCherry-kan) to JW3753, rhlB-YFP strain.

To construct strains OG313, OG456 and OG315, expressing Hfq-mCherry in the background of *elaB*, *yqjD* or *tmaR* deletion, respectively, the respective knockout strains from the Keio collection[65] were infected with PI phage. P1 lysates were prepared from each of the three infected strains, followed by their transduction to OG172 (MG1655 Hfq-mCherry) strain.

To construct strain OG331, *tmaR* deletion in MG1655 background, the same P1 lysate of Δ*tmaR* cells was used to infect MG1655 cells. pCP20 plasmid was used to remove the kanamycin cassette resulting in the construction of the OG357 strain.

To construct strain OG62 and OG358, a *minD*-G262D point mutation in MG1655 background or Δ*tmaR* deletion, respectively, the kanamycin cassette was amplified from pKD4 plasmid with homology to the min locus, followed by an introduction to χ1488 strain, which contains the pKD46 plasmid. The verified cells were grown at 42ºC and tested for loss of pKD46. P1 lysate was prepared, followed by transduction to MG1655 and OG357.

Strain OG561, expressing a truncated *tmaR* derivative deleted for helix 2, was constructed by two overlapping PCR amplifications of part of the *tmaR* gene or of the sequences following the gene, which were ligated using Gibson assembly. The assembled sequence was amplified and introduced into MG1655 using positive and negative selection.[66] The TS-mYFP-TmaR-helix1[29] was amplified by the primers F-helix1-1 and R-helix1-1. The sequence following the *tmaR* gene was amplified from MG1655 chromosome using primers F-helix1-2 and R-helix1-2. After validation by sequencing, the resulting strain was transduced by a P1 lysate of the Hfq-mCherry-kan fragment.

To construct strain OG570, expressing a truncated *tmaR* derivative deleted for helix 1, Helix 2 of TmaR was amplified with primers that contain the sequences before and after the *tmaR* gene (50 bp before and after the gene). The amplicon was then introduced into MG1655, replacing the *tmaR* gene via homology recombination, using positive and negative selection.[66] After validation by sequencing, the resulting strain was transduced by a P1 lysate of the Hfq-mCherry-kan fragment.

Plasmid construction

The pBAD18-Hfq-mCherry plasmid was constructed by amplifying the *hfq* gene including the three putative promoters preceding it from MG1655 using primers that introduced ClaI and SacI sites at the 5′ and-3′ ends, respectively. The amplified fragment was ligated to pBAD18LL-mCherry, which was cleaved by ClaI and SacI.

pBAD18-mCherry plasmid, with the regulatory elements of the *hfq* gene, was constructed by inverse PCR reaction on pBAD18-Hfq-mCherry plasmid using forward phosphorylated primer from the beginning of the mCherry ORF and a reverse primer from the end of *hfq* promoter, followed by closure of the amplified fragment by ligation.

Plasmids containing truncated *hfq* [*hfq*(Nter1-65aa) and *hfq*(Cter73-102aa)], fused to mCherry, which include the *hfq* gene regulatory elements, were constructed using inverse PCR reaction on a pBAD18-Hfq-mCherry plasmid. These amplified plasmid fragments were self-ligated to create pBAD18-HfqNter-mCherry and pBAD18-HfqCter-mCherry, respectively.

The pQE80L-Hfq-mCherry plasmid was constructed as followed: pQE80L-Hfq-his backbone was amplified between the end of the hfq gene and the HindIII site on the plasmid. The mCherry fragment was amplified from pBAD18-Hfq-mCherry with primers containing homology to the pQE80L-Hfq-his backbone. The two fragments were digested by DpnI and ligated by Gibson assembly.[67]

pET15b-Hfq-mCherry and pET15b-mCherry plasmids were constructed by amplifying the fragments encoding Hfq-mCherry and mCherry from pQE80L-Hfq-mCherry using reverse primer at the end of mCherry gene and forward primer at the beginning of either *hfq* or *mCherry* genes, respectively, all containing homology to the pET15b vector sequence. The amplified vector and the PCR mCherry-containing inserts were digested by DpnI. The Hfq-mCherry and mCherry fragments were ligated to pET15b vector using Gibson assembly to create pET15b-Hfq-mCherry and pET15b-mCherry plasmids, respectively.

pZE12-TmaR-Y79F and pZE12-TmaR-Y51F plasmids were constructed using two overlapping PCR products that were combined by Gibson assembly. The first amplicon was amplified from pZE12-TmaR,[29] using the primers F-pZE12-TmaR and R-pzE12 that annealed to the N and C termini of the *tmaR* gene, respectively. The second amplicon was amplified from TS-TmaRY79F or TS-TmaRY51F[28] using F-TS-TmaR and R-TS-TmaR primers, respectively.

The pZA14-TmaR-FLAG plasmid was constructed by amplifying *tmaR* gene from MG1655 chromosome using primers F-KpnI-FT-yeeX and R-yeeX-SC-ClaI, containing FLAG tag and introducing KpnI and ClaI restriction sites at the 5′ and-3′ ends, respectively. The amplified fragment and pZA14 vector were both digested using the indicated enzymes followed by ligation.

Fluorescent microscopy

MG1655 and its derivatives were grown overnight in LB medium with the appropriate antibiotics at 30°C, diluted 100-fold in fresh medium and grown to exponential phase. When indicated, protein expression was induced. Cells were placed on an agarose pad with uncoated coverslips and were imaged using Nikon Eclipse Ti-E inverted microscope equipped with Perfect Focus System (PFS) and ORCA Flash 4 camera (Hamamatsu photonics). Images were processed and two-dimensional (2D) deconvolution was performed using NIS Elements-AR software.

Immunostaining

Immunostaining for Hfq-FLG was conducted as described previously.[17] Briefly, HM34 (MG1655 Hfq-FLAG) and OG185 (MG1655 Δ*hfq*) cells were grown overnight in LB at 30°C. Cells were dehydrated in 80% methanol and pelleted down at low speed (3000 g for 15 s). The cells were resuspended in ice-cold 100% methanol and stored at 4°C for one hour. Cells were pelleted at low speed and resuspended in GTE (Glucose-Tris-EDTA buffer). Fresh lysozyme was added to the cells and they were fixed on poly-L-lysine-coated coverslips. After a short incubation, the suspension was removed, the slides were washed thrice with PBS and dried at room temperature. The slides were rehydrated with PBS and blocked with 2% BSA in PBS for 20 min. The slides were stained with an Anti-FLAG antibody for 1 h. The slides were washed multiple times with PBS and stained with Alexa Fluor 594, Anti-Mouse IgG (H + L) for 1 h in the dark. The coverslips were mounted on agar pads made of 1% agarose in 1× PBS and imaged as described above.

Fluorescence recovery after photo bleaching (FRAP)

For FRAP microscopy, Nikon A1R confocal microscope equipped with Apochromat 60X objective (numeric aperture 1.4) was used. Photobleaching was done over the area in which the Hfq cluster is localized. Recovery was measured every 10 s for a total period of

10min. Mean fluorescence intensity was normalized to the total fluorescence intensity for each ROI after bleaching. Images were analyzed using the NIS Elements AR module.

Protein purification

For purification of Hfq-mCherry and mCherry, these proteins were overexpressed in BL21(DE3) cells from pET15b-Hfq-mCherry and pET15b-mCherry, respectively. Five hundred (500) mL culture were harvested and lysed using glass beads and a Mixer Mill MM400 instrument. The lysates were loaded on Nickel (Ni-NTA) gravity column and treated as suggested by the manufacturer. Proteins were eluted using 250 mM imidazole and were verified for their concentration and purification.

Untagged Hfq was purified as described before[68] with several adaptions. Briefly, an overnight culture of BL21(DE3) cells carrying pET-15b-Hfq was diluted 1:100 in 1 L of fresh LB and grown to OD_{600} = 0.6. IPTG (1 mM final concentration) was then added, and growth continued for 3 more hrs. The cells were pelleted, washed with PBS, and resuspended in lysis buffer [50 mM Tris, 1.5 M NaCl, 250 mM $MgCl_2$,1 mM β-mercaptoethanol, PMSF, DNase I (0.1 mg/mL) and 1M $MgCl_2$]. Cells were then lysed by Mixer Mill MM400 using glass beads. The Supernatant was collected, incubated at 85°C for 45 min, centrifuged again and treated with RNase A (30 μg/mL) for 1 h at 37°C. The RNase A-treated lysate was loaded on Nickel (Ni-NTA) gravity column and treated as suggested by the manufacturer. Proteins were eluted using 250 mM imidazole and were verified for their concentration and purification.

His-GFP-TmaR was purified as described before.[29] Shortly, an overnight culture of BL21(DE3) carrying pET-GFP-TmaR was diluted 1:100 in 1 L of fresh LB, supplemented with 0.1mM IPTG, and grown until OD_{600} = 0.6. The cells were then centrifuged for 10 min at 4500 RPM at 4ºC in Thermo Sorvall RC6+ and stored at −80ºC. Cells were resuspended in 8 mL PBS containing 10 mM imidazole and lysed by Mixer Mill MM400 using glass beads. The lysate was loaded on Nickel (Ni-NTA) gravity column and treated as suggested by the manufacturer. Proteins were eluted using 250 mM imidazole and were verified for their concentration and purification.

In vitro liquid-liquid phase separation assays

Hfq-mCherry protein aliquots were thawed on ice. All experiments were conducted in 50 mM HEPES and 150 μM NaCl unless stated differently. The purified Hfq-mCherry protein concentration used for all experiments was 0.1 μM unless indicated differently. For all *in vitro* assays, proteins were diluted 1:200 in the indicated buffer, according to the specific experiment. PEG 6 kDa, PEG 8 kDa, NaCl, Hexanediol, poly(A), poly(U), labeled RNA or purified TmaR protein were added to the HEPES-NaCl buffer before the addition of the protein. Protein was added to the indicated tube and transferred to a Lab-Tek™ Chambered Cover glass (Thermo Scientific). All images were taken and analyzed as described above.

In vitro transcription and labeling

SgrS sRNA and *ptsG* mRNA were transcribed and labeled using the HighYield T7 AF488 RNA Labeling Kit (Jena Bioscience) as recommended by the manufacturer, using the respective amplified genes in MG1655 chromosome as templates. For DNA template removal, Turbo™DNAse (Thermo Fisher) was used. RNA was then purified and concentrated using the RNA Clean & Concentrator Kits (Zymo Research). Finally, the concentration and purity of the RNA were measured by Qbit and NanoDrop, respectively. Defined concentrations of labeled RNA were used for the *in vitro* microscopy experiments.

Co-immunoprecipitation for detecting Hfq-TmaR interaction

Cells of OG357 containing plasmid pZA14-tmaR or the empty vector pZA14, were grown overnight with the required antibiotics and without the addition of IPTG. Cell density was measured, and an equal number of cells was harvested by centrifuging at 10,000 rpm for 10 min at 4°C. The pelleted cells were resuspended in 1 mL PBS and transferred to glass tubes. Cross-linking was applied by the addition of formaldehyde fresh solution to a final concentration of 1% for 20 min and shaking at room temperature. Glycine, at a final concentration of 250 mM, was added to stop the reaction, followed by additional incubation for 10 min. Cells were pelleted down and resuspended in TBS containing 1 mM AEBSF, 0.5% sarkosyl and DNase I, followed by lysis via Mixer Mill MM400 using glass beads. Anti-DYKDDDDK G1 Affinity Resin (GenScript) was equilibrated in TBS. 60 μL bead slurry was resuspended twice in 500 μL TBS (ice-cold) and centrifuged at 6,000 g for 30 s at 4°C. The cell lysate was added to the equilibrated Anti-DYKDDDDK G1 Affinity Resin and incubated with gentle end-over-end mixing for 2 h at 4°C. The tube was centrifuged at 6,000 g for 30 s at 4°C, and the supernatant was discarded. The pellet was washed trice with 1 mL of TBS (ice-cold). Beads were resuspended in 30 μL TBS, and 30 μL 2x SDS sample buffer was added. The resuspended beads were incubated at 95°C for 5 min to dissociate the immunocomplexes from the beads and revert the cross-linking. The beads were pelleted by centrifugation at 8,000 g for 1 min, and SDS-PAGE was performed with the supernatants. The blot was reacted with an anti-mCherry antibody to detect the presence of Hfq-mCherry in the eluted fraction.

Fluorescence *in situ* hybridization (FISH)

FISH was performed essentially as described previously.[17,69] Briefly, for nutrient deprivation MG1655 and OG331 (MG1655 Δ*tmaR*) were grown overnight in LB at 30°C. For envelope stress, the same cells were grown to mid-log phase and stress was induced as described above. Cells were cross-linked by adding formaldehyde to a final concentration of 3.7–4%, followed by incubation for 15 min at room temperature and 30 min on ice. Cells were then pelleted at 4,000 rpm for 7 min, washed thrice with nuclease-free

PBS and resuspended in GTE (50 mM glucose, 10 mM EDTA - pH 8, 20 mM Tris-HCl - pH 7.5). Fresh lysozyme was added to a final concentration of 20 μg/mL for 1min and 20 μL cells were immediately added to each well on a FISH slide pre-treated with poly-L-lysine. The slides were washed thrice with PBS, once with chilled 80% methanol and chilled acetone, and air-dried at 37°C for 5 min. Next, the slides were washed with chilled 50% ethanol and air-dried at 37°C for 5 min. The slides were then washed twice with SSCT (0.03 M sodium citrate, 0.03 M NaCl, and 0.1% Triton X-100) and prehybridized with 2X SSCT + 50% formamide for 30 min at 37°C. For hybridization, 1.5 μL of Alexa 488 labeled probe (HyLabs) and 15 μL of hybridization buffer (3xSSC, 50% formamide, 10% dextran sulfate and 40 U RNase inhibitor) were added to each well and covered with coverslip. The slides were incubated at 94°C for 2 min followed by overnight incubation at 55°C in a dark hydrated condition. On the next day, the slides were washed twice with SSCT + 50% formamide for 30 min at 37°C, once with 2X SSCT + 25% formamide for 10 min at room temperature, thrice with 2X SSCT for 10 min at room temperature, and once with PBS for 10 min at room temperature. The cells on the slides were crosslinked again by adding 3.7% formaldehyde and incubated for 30 min at room temperature. Next, the slides were washed once with PBS at room temperature, 80% methanol at room temperature, followed by three washes with PBS at room temperature. The slides were air-dried and 15 μL PBS was added to each well and sealed gently with a coverslip. Finally, the cells were imaged as described above.

Minicells purification

To examine the polar sRNA content, minicells were purified from OG62 and OG358 essentially as described previously.[17,57] Briefly, cells grown to exponential phase were harvested by low-speed-centrifugation. The pellet, enriched with the rod cells was washed twice with 50 mM Tris-Cl to purify the rod cells. The supernatant was centrifuged at low-speed several times until there was no visible pellet. Finally, the minicells in the supernatant were pelleted. The purification of the rod cells and minicells was verified using phase microscopy.

RT-qPCR

Total RNA was isolated and RNA concentrations were determined using a NanoDrop machine (NanoDrop Technologies). DNA was degraded by DNase treatment and an equal concentration of 1 μg of DNA-free RNA was measured by Qubit fluorimeter (Invitrogen). The DNA-free RNA was then used for cDNA synthesis. cDNA was quantified by real-time PCR using SYBR-green mix in CFX Connect Real-Time System (Bio-Rad) in a 96-well plate module according to manufacturer instructions. Specific primers were designed for each target gene and the expression of each gene was normalized to the gyrA level. The relative amount of cDNA was calculated by comparative Ct method, and ΔCt was measured in triplicate. CFX maestro analysis software was used for conducting the analysis.

GFP reporter assay

The GFP reporter assay was done as described previously using the same constructs[5,33] with some changes. Briefly, the wild-type strain (MG1655) or its derivatives, OG172(MG Hfq-mCherry), or OG185 (MG Δ*hfq*) were transformed with a target-GFP reporter plasmid and with an sRNA overexpressing plasmid. The experiments were compared to control plasmids: a non-GFP plasmid (pXG0) and sRNA control plasmids (pJV300). Cultures of biological replicates were grown overnight at 30°C in LB supplemented with ampicillin and chloramphenicol. Fluorescence was measured using the Synergy H1 plate reader (BioTek). The level of regulation was determined by subtracting auto-fluorescence and calculating the ratio between the fluorescence level in an sRNA overexpressing strain and a control plasmid-carrying strain.[33]

Growth test

The growth of OG172 (MG1655 Hfq-mCherry) strain was compared to that of MG1655 (wild type) and OG185 (*hfq* deletion strain) as follows. An overnight culture was diluted 1:100 in fresh LB and 180 μL were transferred to 96-well microplates (Nunc). The cells in the plate were then grown for 3.5 h at 30ºC without shaking. Absorbance at 600 nm was measured every 7 min after shaking for 5 s in a 96-well plate reader (Bio Tek, Synergy H1). The experiment was conducted in 3 biological replicates and 3 technical replicates for each biological replicate.

Western blot analysis

An equal number of cells from each strain were collected. Proteins were separated on SDS-polyacrylamide gels, which were subjected to Western blot analysis as described previously.[69] The membrane was stained with Ponceau S to evaluate similar protein loading. The membrane was then probed with α-mCherry (Abcam) for the detection of Hfq-mCherry. Signals were visualized by the ECL system (Biological industries).

Semi-native Western blot analysis

Cells were grown to the indicated growth phase and an equal number of cells were collected from each strain by centrifugation. To examine Hfq under semi-native conditions (in order to capture Hfq hexametric form), we resuspended cell pellets in lysis buffer without any detergents (50 mM NaH_2PO_4, 300 mM NaCl) followed by lysis using Mixer Mill MM400 and glass beads. Protein samples were mixed in a 1:1 ratio with semi-native loading buffer (containing 100 mM Tris pH 6.8, 0.5% SDS, 0.2% Bromophenol Blue, 20% Glycerol and no reducing agents) and were not boiled. Proteins were separated on a 12–20% gradient precast gel (Bio-Rad), followed by traditional Western blot analysis as described above.

Promoter GFP assay

Overnight cultures of WT and *tmaR* deletion harboring plasmids overexpressing GFP from the promoters of *ompC*, *ompA*, *ompX*, *gadX* and *rpoS* genes. Cultures were diluted 1:100 and grown to mid-logarithmic phase. High osmolarity stress was applied as described above, and cells were grown for 2 more hours. Samples were transferred to Greiner 96 well cell culture microplate μclear®, black (655090) after centrifugation and suspension with PBS. OD_{600} and GFP were measured using the Synergy H1 plate reader (BioTek). GFP values were normalized to the OD_{600} of the sample. The experiment was conducted in three biological replicates and two experimental replicates.

Electro-mobility shift assay (EMSA)

EMSA was conducted as described previously[56] with some changes. Briefly, 28 nM of untagged RNase-free Hfq, purified as described above, were incubated for 15 min with labeled RNAs (100 nM Cy5-DsrA and 50 nM Cy3-*rpoS*, Sigma-Aldrich). After incubation, samples were subjected to electrophoresis in a 0.75 mm thick 20% polyacrylamide (29:1) gel (150mM Tris-HCl, pH 8.0). Electrophoresis was conducted at room temperature at 70 V (25mM Tris and 250mM glycine) for 4 h. Gels were imaged using a ChemiDoc MP Imaging System (Bio-Rad). Bands were quantified using the ImageJ software.

QUANTIFICATION AND STATISTICAL ANALYSIS

All the experiments conducted for this study were performed in at least three biological replicates, and the data from each experiment was expressed as mean ± SEM (Standard Error of the Mean). Analysis of variance was performed using non-parametric test, as indicated for each analysis. p values < 0.05 were considered significant. All statistical analyses were performed using the GraphPad Prism software version 6 (GraphPad Software, San Diego, California).